Acta Pharmaceutica Sinica B 2025;15(1):151−167

Chinese Pharmaceutical Association
Institute of Materia Medica, Chinese Academy of Medical Sciences

Acta Pharmaceutica Sinica B

www.elsevier.com/locate/apsb
www.sciencedirect.com

ORIGINAL ARTICLE

Akkermansia muciniphila-derived acetate activates the hepatic AMPK/SIRT1/PGC-1α axis to alleviate ferroptosis in metabolic-associated fatty liver disease

Aoxiang Zhuge[a,†], Shengjie Li[b,†], Shengyi Han[b], Yin Yuan[b], Jian Shen[b], Wenrui Wu[b], Kaicen Wang[b], Jiafeng Xia[b], Qiangqiang Wang[b], Yifeng Gu[b], Enguo Chen[a,*], Lanjuan Li[b,c,d,*]

[a]*Department of Pulmonary and Critical Care Medicine, Sir Run Run Shaw Hospital, School of Medicine, Zhejiang University, Hangzhou 310016, China*
[b]*State Key Laboratory for Diagnosis and Treatment of Infectious Diseases, National Clinical Research Center for Infectious Diseases, National Medical Center for Infectious Diseases, Collaborative Innovation Center for Diagnosis and Treatment of Infectious Diseases, the First Affiliated Hospital, Zhejiang University School of Medicine, Hangzhou 310003, China*
[c]*Research Units of Infectious Disease and Microecology, Chinese Academy of Medical Sciences, Beijing 100730, China*
[d]*Jinan Microecological Biomedicine Shandong Laboratory, Jinan 250000, China*

Received 15 July 2024; received in revised form 3 August 2024; accepted 6 September 2024

KEY WORDS

Metabolic-associated fatty liver disease;
Ferroptosis;
Lipid peroxidation;
Akkermansia muciniphila;
Acetate;
Adenosine 5′-monophosphate-

Abstract Emerging evidences have indicated the role of ferroptosis in the progression of metabolic-associated fatty liver disease (MAFLD); thus, inhibiting ferroptosis is a promising strategy for the development of MAFLD therapeutics. Recent studies have demonstrated the antioxidative effect of the gut commensal bacterium *Akkermansia muciniphila* (*A. muc*); however, whether it can alleviate ferroptosis remains unclear. The current study indicates *A. muc* intervention efficiently reversed high-fat high-fructose diet (HFHFD)-induced lipid peroxidation and ferroptosis in the liver. These beneficial effects were mediated by activation of the hepatic AMPK/SIRT1/PGC-1α axis, as evidenced by the finding that AMPK deficiency abrogated the amelioration of lipid peroxidation *in vitro* and *in vivo*. Furthermore, the short-chain fatty acids (SCFAs) were enriched upon *A. muc* treatment, and acetate

*Corresponding authors.
E-mail addresses: ljli@zju.edu.cn (Lanjuan Li), 3195024@zju.edu.cn (Enguo Chen).
†These authors made equal contributions to this work.

Peer review under the responsibility of Chinese Pharmaceutical Association and Institute of Materia Medica, Chinese Academy of Medical Sciences.

https://doi.org/10.1016/j.apsb.2024.10.010

activated protein kinase; Polyunsaturated fatty acid synthesis

was identified as a key activator of hepatic AMPK signalling. Mechanistically, microbiota-derived acetate was transported to the liver and metabolized to adenosine monophosphate (AMP), which triggered AMPK activation. Furthermore, a colonization assay in germ-free mice confirmed that *A. muc* mediated antiferroptotic effects in the absence of other microbes. These data indicated that *A. muc* exerts antiferroptotic effects against MAFLD, at least partially by producing acetate, which activates the hepatic AMPK/SIRT1/PGC-1α axis to alleviate ferroptosis *via* the inhibition of polyunsaturated fatty acid (PUFA) synthesis.

1. Introduction

Metabolic-associated fatty liver disease (MAFLD), previously known as nonalcoholic fatty liver disease (NAFLD), encompasses a disease spectrum that progresses from simple steatosis to nonalcoholic steatohepatitis (NASH)[1,2]. NASH is a more complex stage, manifested by severe steatosis, hepatocellular damage, inflammation, and fibrosis, which may lead to cirrhosis, hepatocellular carcinoma (HCC), and end-stage liver disease[3]. Hepatocyte death is a key event in NASH progression, which subsequently triggers immune cell recruitment, compensatory hepatocyte proliferation, and hepatic stellate cell activation, ultimately progressing to fibrosis[4]. To date, various types of hepatocellular death in MAFLD, including apoptosis, necrosis, necroptosis, and pyroptosis, have been widely investigated, and each type of cell death can stimulate specific responses through different mechanisms[5]. Ferroptosis, a specific type of regulated cell death resulting from the accumulation of iron-dependent lipid peroxides, has recently been recognized to participate in the pathogenesis and progression of metabolic diseases and even liver fibrosis[6-10], as evidenced by elevated peroxidation biomarkers, namely, malondialdehyde (MDA) and 4-hydroxinonenal (4-HNE)[11], as well as liver siderosis, in NASH patients[12]. Because the antioxidant vitamin E or ferroptosis inhibitors, such as Trolox and deferiprone, can suppress NASH progression[13,14], inhibiting lipid peroxidation and ferroptosis is an emerging strategy for NASH therapeutics.

Currently, there are no approved medical treatments for MAFLD, emphasizing the need to develop novel strategies involving other targets[15]. Notably, the role of the gut microbiota in MAFLD pathogenesis and development has been well verified, as exemplified by microbial alterations in MAFLD patients in several human cohort-based studies[16-18]. Microbiota-derived noninvasive diagnostic tools with considerable diagnostic efficiency have been established[19,20], whereas microbiota-targeted therapies need further investigation to specifically link the gut microbiota with disease pathogenesis. Existing microbial strategies mainly target dysfunctional gut microbiota composition (antibiotics, prebiotics, probiotics, synbiotics, phages, and faecal microbiota transplantation) or gut microbial metabolism (postbiotics, engineered microbes, and specific metabolites)[21,22]. *Akkermansia muciniphila* (*A. muc*), a mucin-degrading microbe primarily isolated from human stool, has been recognized as a next-generation probiotic with several beneficial effects on metabolic disorders[23-26]. The mechanisms of *A. muc*-mediated beneficial effects on MAFLD may include a reduction in carbohydrate absorption[27], the regulation of intestinal immunity[28], the regulation of barrier functions[29], and the modulation of gut−liver L-aspartate metabolism[30]. Recent studies have demonstrated the antioxidative effect of *A. muc* against oxidative damage[30-32], which is a key manifestation of lipid peroxidation. However, it remains unknown whether *A. muc* could alleviate MAFLD-related lipid peroxidation and ferroptosis, and the underlying specific mechanism is unclear, thereby requiring further investigation.

Synergy between *A. muc* and prebiotics has been reported in the treatment of metabolic diseases[33]. Previously, we reported that *A. muc* increases faecal levels of short-chain fatty acids (SCFAs)[34,35], which are primary products fermented by gut microbes from dietary prebiotics[36]. SCFAs that participate in colon energy metabolism are absorbed by colonocytes; those not metabolized in the colon are transported in the portal circulation, and some of them are used as energy substrates for hepatocytes[37,38]. Additionally, SCFAs, notably acetate, propionate, and butyrate, exhibit great potential to ameliorate metabolic disorders[39-41]. These previous studies indicated that the *A. muc*-mediated beneficial metabolic effects may be, at least partially, related to gut microbiota-derived SCFAs.

The present study established a long-term high-fat high-fructose diet (HFHFD)-fed mouse model to mimic clinical NASH profiles as previously reported[42]. The present aims were to elucidate the role of lipid peroxidation and ferroptosis in NASH progression, as well as to investigate whether *A. muc* treatment could undermine this pathological process. Further, the present study aimed to identify the activated pathway and key microbiota-derived metabolites that mediate the antiferroptotic effect of *A. muc*. The present results demonstrated that *A. muc* administration efficiently alleviates lipid peroxidation and ferroptosis during NASH progression, accompanied by SCFA enrichment in the intestine and liver. Importantly, we identified *A. muc*-derived acetate as a key metabolite that activates the hepatic AMPK/SIRT1/PGC-1α pathway to protect against lipid peroxidation and ferroptosis in MAFLD mice *via* the inhibition of PUFA synthesis.

2. Materials and methods

2.1. Bacterial strains and culture conditions

The *A. muc* strain (ATCC BAA-835, received from Dr. Wenrui Wu) was cultured in modified brain heart infusion (BHI) medium at 37 °C anaerobically (AW300SG, Electrotek, Cookley, Kidderminster, England) for 48 h. The modified BHI medium consisted of BHI broth (37 g/L, Oxiod Ltd., Hampshire, England), mucin (0.5%, Sigma−Aldrich, St. Louis, MO, USA), and L-cysteine (0.05%, Sigma).

The *Bifidobacterium longum* R0175 strain (*B. longum*) purchased from Lallemand (Quebec, Canada) was cultured in trypticase-phytone-yeast (TPY) broth (RiShui, Qingdao, China) at 37 °C anaerobically for 24 h.

The *Escherichia coli* (*E. coli*) strain (ATCC 25922) was cultured in Luria−Bertani (LB) broth (Oxiod Ltd.) at 37 °C aerobically for 24 h.

The *Lactobacillus reuteri* DSM17938 strain (*L. reuteri*) was cultured in DeMann, Regosa, Sharpe (MRS) broth (Oxiod Ltd.) at 37 °C anaerobically for 24 h.

To harvest bacteria, *A. muc* was harvested *via* centrifugation at 10,000 rpm for 10 min at 4 °C, and *B. longum*, *E. coli* and *L. reuteri* were harvested *via* centrifugation at 4000 rpm for 10 min at 4 °C. A high-speed centrifuge was applied for harvesting bacteria (CR22N, Eppendorf, Hamburg, Germany).

2.2. Animal model and treatment

Specific pathogen-free C57BL/6J mice (6 weeks old) purchased from the SLAC laboratory (Shanghai, China) were acclimatized for one week before treatment. All the mice were housed at room temperature with a controlled 12-to-12-h light/dark cycle and had free access to food and water. All the mice involved in the experiments were male C57BL/6J mice aged 6 weeks, unless otherwise stated.

For the *A. muc* treatment model, the mice were randomly divided into the following two subgroups: (a) mice fed a HFHFD (60 kcal% fat in feed, D12492, Research Diet; 23.1 g of fructose and 18.9 g of glucose in 1 L of drinking water, Sigma)[43] for up to 20 weeks and treated with *A. muc* (treatment group) or an equivalent volume of normal saline (positive control group); and (b) mice fed a normal control diet and treated with normal saline (negative control group). *A. muc* was harvested and resuspended in anaerobic normal saline and given to the treated mice (10^9 CFU per mouse) twice a week by oral gavage.

For the MAFLD progression model, the mice were fed a HFHFD for 0, 4, 8, 12, or 16 weeks before sacrifice.

For the short-chain fatty acid treatment model, the mice were fed a HFHFD for up to 8 weeks and treated with vehicle, sodium acetate (0.6 g/kg), sodium propionate (0.6 g/kg), or sodium butyrate (0.6 g/kg) daily starting at Week 4 for 4 weeks.

For the SCFA-producing microbe treatment model, the mice were fed a HFHFD for up to 8 weeks and treated with equivalent volumes of vehicle, *A. muc*, *B. longum*, *E. coli*, or *L. reuteri* (10^9 CFU per mouse) daily starting at Week 4 for 4 weeks.

For the AMPK knockdown model, the mice were injected with 1.5×10^{11} vg shPrkaa1 or an equivalent volume of shCtrl *via* the tail vein and fed a HFHFD for up to 8 weeks. Starting at Week 4, the mice were gavaged daily with *A. muc* (10^9 CFU per mouse) or an equivalent volume of vehicle for 4 weeks.

For the faecal microbiota transplantation (FMT) model, the mice were pretreated with an antibiotic cocktail for 7 days, fed a HFHFD, and gavaged with microbiota suspensions daily for up to 2 weeks.

For the germ-free (GF) mouse model, male ICR mice aged 6−8 weeks were fed a HFHFD for up to 8 weeks and colonized with *A. muc* (10^9 CFU per mouse) three times in the first week.

All procedures were performed in strict accordance with the 2011 National Institutes of Health Guide for the Care and Use of Laboratory Animals. All animal experiments were approved by the Animal Ethics Committee of the First Affiliated Hospital School of Medicine, Zhejiang University (Approval No. 2021-1408).

2.3. Faecal microbiota transplantation

Stool samples from *A. muc*-treated mice were collected in sterile containers at Week 19. FMT was conducted as previously described with some modifications[44]. Briefly, 0.5 g of stool was resuspended in 1 mL of sterile saline and centrifuged at 500 rpm at 4 °C (5425R, Eppendorf) for 1 min to harvest the microbial supernatant. Mice were subjected to one week of microbiota purification *via* an antibiotic cocktail, which included 100 mg/kg vancomycin, 200 mg/kg neomycin sulfate, 200 mg/kg metronidazole, and 200 mg/kg ampicillin. The mice were then fed a HFHFD and gavaged with 200 μL of microbial supernatant daily for 2 weeks to transfer the microbiota.

2.4. Cell culture and treatment

The human hepatocellular carcinoma cell line HepG2 (ATCC HB-8065) and the mouse hepatocyte cell line AML12 (ATCC CRL-2254) were cultured in Dulbecco's modified Eagle's medium (DMEM, Gibco, MD, USA) supplemented with 10% foetal bovine serum (FBS, Inner Mongolia Opcel Biotechnology Co., Ltd., Neimenggu Nei, China) and 1% penicillin/streptomycin (Beyotime, Shanghai, China) in 37 °C with 5% CO_2.

To investigate the effects of SCFAs on hepatocellular AMPK activation, cells were cultured with 0.5 mmol/L sodium acetate, 0.5 mmol/L sodium propionate, and 0.5 mmol/L sodium butyrate with or without 2 μmol/L erastin for 24 h.

To investigate whether SCFAs alleviate hepatocellular ferroptosis by activating AMPK, cells were cultured with 0.5 mmol/L sodium acetate under 2 μmol/L erastin challenge for 24 h in the presence or absence of pretreatment with 2 μmol/L Compound C for 12 h.

2.5. Cell viability assay

An enhanced Cell Counting Kit-8 (CCK-8; Beyotime) was used to measure cell viability. AML12 cells were seeded in 96-well plates at a density of 5000 cells per well and cultured with different treatments. The cells were then incubated with the CCK8 assay mixture for 2 h, and the absorbance was measured at 450 nm. For each condition, six independent biological duplicates were assessed.

2.6. Insulin resistance assay

The intraperitoneal glucose tolerance test (IGTT) was performed 1 week before sacrifice. In brief, the mice were fasted for 15 h and then administered with 2 g/kg glucose by intraperitoneal injection. Blood glucose levels were evaluated at 0, 15, 30, 60, 90, and 120 min after injection with a glucometer (Roche, Basel, Switzerland). The serum levels of insulin were measured with a commercial ELISA kit (Invitrogen).

2.7. Lipid peroxidation assay

The lipid peroxidation levels in HepG2 cells treated with erastin with or without acetate and Compound C were evaluated *via* the use of C11-BODIPY (Invitrogen). Briefly, cells were seeded at a density of 10,000 cells per well in a 24-well plate and subjected to different treatments. After incubation with 2 μmol/L C11-BODIPY for 20 min at 37 °C, the stained cells were washed twice with cold PBS and imaged *via* a fluorescence microscope (Olympus, Tokyo, Japan).

2.8. Histopathological analysis

Liver sections were collected at sacrifice and fixed in 10% paraformaldehyde for 24 h. The samples were then embedded in paraffin and cut into 2 μm-thick sections, which were stained with haematoxylin and eosin (H&E) and Oil Red O for further analyses.

To evaluate the degree of MAFLD progression, the NAFLD activity score (NAS) system was utilized as previously described[45].

2.9. Quantification of reactive oxygen species (ROS) and dihydroethidium (DHE) staining

ROS in the liver and ileum were quantified *via* an ROS quantification kit (Biolab, Beijing, China) according to the manufacturer's instructions. Frozen sections of the liver and ileum fixed with OCT (10 μm) were stained with DHE (Haoke Biotechnology, Wuhan, China). Images of the stained sections were captured *via* the Nano-Zoomer Digital Pathology system (Hamamatsu Photonics, KK, Japan) at 400 × and 200 × magnification.

2.10. Liver ELISA

The liver levels of malondialdehyde (MDA), glutathione (GSH), L-aspartate, ATP, adenosine monophosphate (AMP), and acetyl Co-A were quantified *via* commercial ELISA kits following the manufacturer's instructions (Supporting Information Table S1). Briefly, liver sections were homogenized and centrifuged to harvest the supernatant for further measurements. The AMP-to-ATP ratios were determined using the AMP and ATP concentrations in the supernatants obtained from the same liver section.

2.11. Immunohistochemistry analysis

Liver samples were collected in 10% formaldehyde for 24 h and embedded in paraffin. The paraffin-embedded tissue was then cut into 4 μm thick sections and incubated with primary antibody (Boster, Wuhan, China), followed by incubation with horseradish peroxidase-conjugated secondary antibody (Beyotime, Shanghai, China) and 3,3′-diaminobenzidine (Beyotime) for specific visualization.

2.12. Fluorescence in situ hybridization (FISH) and immunofluorescence staining

Sample collection and fixation for FISH were performed as previously described[46]. Briefly, distal colon sections containing a faecal pellet were fixed in methacarn solution (containing 60% methanol, 30% chloroform, and 10% acetic acid) for 48 h, followed by a series of rinses (methanol for 35 min, ethanol for 30 min, and xylene for 25 min). The tissue was then embedded in paraffin, cut into 4 μm thick sections, and deparaffinized for FISH.

FISH was performed as previously described[46]. In brief, deparaffinized colon sections were initially incubated with 10 ng/μL bacterial FISH probe diluted in hybridization buffer (0.9 mol/L NaCl, 20 mmol/L Tris−HCl, 0.01% sodium dodecyl sulphate, and 10% formamide) at 50 °C for 20 min in the dark[47]. After three PBS washes, the sections were subsequently incubated with 1 mg/mL FITC-UEA1 (Sigma) at 4 °C for 1 h in the dark. After an additional wash, the samples were mounted in mounting medium (containing DAPI, Beyotime). The stained samples were scanned *via* a fluorescence confocal microscope (Zeiss, Jena, Germany). The fluorescently labelled DNA probes used are listed in Supporting Information Table S2.

2.13. RNA extraction and real-time quantitative PCR

RNA extraction was conducted *via* an RNeasy Mini Kit (Qiagen, Germantown, MD, USA) following the manufacturer's protocol. A PrimeScript Master Kit (TaKaRa, Kyoto, Japan) was used to synthesize cDNA. Relative gene expression levels were quantified *via* a SYBR Green Premix qPCR Kit (Takara) with a VIIA7 real-time PCR system (Applied Biosystems, Foster, CA, USA). Each template was run in duplicate and normalized to the *Gapdh* control gene. The primers used are listed in Table S2.

2.14. Western blot analysis

Protein extraction was conducted by homogenizing the tissue or cells with RIPA lysis buffer (Beyotime) containing a protease and phosphatase inhibitor cocktail (Beyotime). Protein concentrations were quantified *via* a BCA kit (Beyotime). After separation by sodium dodecyl sulphate polyacrylamide gel electrophoresis (SDS−PAGE), the proteins were transferred to PVDF membranes (Bio-Rad, Hercules, CA, USA) and incubated with specific primary antibodies (Table S1). The PVDF membranes were then incubated with HRP-conjugated secondary antibodies and visualized *via* an enhanced chemiluminescence kit. ImageJ software was used for the analyses. β-Actin was used as a control.

2.15. RNA-seq and gene set enrichment analysis (GSEA)

Mouse hepatic total RNA was extracted *via* TRIzol reagent (Sigma), and the purity of the RNA was quantified *via* a NanoDrop 2000 spectrophotometer (Thermo Scientific) and an Agilent 2100 Bioanalyzer (Agilent Technologies, Santa Clara, CA, USA). For RNA-seq assays, a cDNA library was constructed *via* the TruSeq Stranded mRNA LT Sample Prep Kit (Illumina) according to the manufacturer's instructions. An Illumina HiSeq X Ten platform was used to sequence the libraries, and 150 bp paired-end reads were generated. The raw data were purified in fastq format *via* Trimmomatic[48]. Clean reads were mapped to the human genome (GRCh38) *via* HISAT2[49]. The FPKM of each gene was calculated *via* Cufflinks[50,51], and the read counts of each gene were obtained *via* HTSeq-count[52]. Differentially expressed genes were identified *via* the DESeq (2012) R package with a standard P value < 0.05 and a fold change (FC) > 2 or < 0.5.

Gene set enrichment analysis (GSEA) was conducted *via* the OmicShare website platform (https://www.omicshare.com/tools/home/report/report_gsea.html). Pathway-involved gene sets were downloaded from the KEGG website and FerrDb database (www.zhounan.org/ferrdb/current). For each KEGG biological pathway, involved genes were defined as a gene set, and a ranked list and a 'gene set' permutation type of the gene set were then generated. Gene sets with P values < 0.05 and FDR values < 0.25 were considered statistically significant.

2.16. Ultra-performance liquid chromatography coupled with electrospray ionization and tandem mass spectrometry (UPLC−ESI-MS/MS) analysis for hepatic untargeted lipidomics

Hepatic lipid profiles were characterized *via* UPLC−ESI-MS/MS as previously described[53]. Briefly, 100 mg of the liver sample was mixed with 750 μL of homogenate agent (chloroform:methanol = 2:1, *v/v*), homogenized, and placed on ice for 40 min. Then, 190 μL of ddH_2O was added to the homogenate, vortexed, and centrifuged at 12,000 rpm for 5 min (TGL-16MS, BIORIDGE, Shanghai, China). The lower layer fluid (300 μL) was mixed with 500 μL of the homogenate agent, vortexed, and centrifuged. Finally, 400 μL of the lower layer fluid was concentrated to dryness under vacuum, dissolved in 200 μL

of isopropanol, and filtered through a 0.22 μm filter prior to LC−MS analysis.

2.17. Targeted short-chain fatty acid (SCFA) profiling via UPLC−ESI-MS/MS

The bacterial products, namely, acetic acid, propionic acid, butyric acid, isobutyric acid, pentanoic acid, and isovaleric acid, in mouse stool and liver were quantified *via* UPLC−ESI-MS/MS. Briefly, 50 mg of mouse sample was mixed and homogenized with 300 μL of acetonitrile solution (50% in water, *v*/*v*), ultrasonicated on ice for 10 min, and centrifuged at 12,000 rpm at 4 °C for 10 min (TGL-16MS, BIORIDGE). The supernatant (40 μL) was then transferred into a sample bottle and mixed with 20 μL of 200 mmol/L 3-NPH (in 50% acetonitrile water solution, *v*/*v*) and 20 μL of 120 mmol/L EDC-6% pyridine (in 50% acetonitrile water solution, *v*/*v*) for derivatization. After cooling on ice for 1 min, the mixture was diluted ten times with 10% acetonitrile in water, and 150 μL of the supernatant was filtered through a 0.22 μm filter, removed from the sample bottle, and stored at −80 °C prior to UPLC−ESI-MS/MS analysis. The derivatization of the standard sample was the same as that of the former, except that no dilution step was needed.

2.18. 16S rRNA sequencing and bioinformatics analysis

Bacterial DNA was extracted *via* a DNeasy PowerSoil Pro Kit (Qiagen, CA, USA) and verified *via* NanoDrop (Thermo Fisher Scientific, MA, USA) and agarose gel electrophoresis. PCR was performed to generate amplicons *via* V3−V4 oligonucleotides (343F: 5′-TACGGRAGGCAGCAG-3′; 798R: 5′-AGGGTATCTAATCCT-3′). After amplification, purification, and qualification, sequencing was performed on an Illumina NovaSeq 6000 platform (Illumina Inc., CA, USA) to construct the library.

The sequencing reads were trimmed *via* Trimmomatic software, assembled *via* FLASH software, and clustered into operational taxonomic units (OTUs) *via* VSEARCH software with a 97% similarity cut-off. Finally, the QIIME package was used to select the representative reads.

2.19. Statistical analysis

The Kolmogorov−Smirnov test was used to evaluate the normality of the data. For data with normal distributions, one-way ANOVA with Tukey's test was used to evaluate differences among more than two groups and adjust for multiple comparisons; otherwise, the Kruskal−Wallis test was used. To compare differences between two groups, Student's *t* test was used to analyse pairwise comparisons with a normal distribution; otherwise, the Mann−Whitney *U* test was used. Correlations between two parameters were evaluated *via* Spearman's rank correlation. The data are shown as the means ± standard error of mean (SEM), and a P value < 0.05 was considered statistically significant.

3. Results

3.1. A. muc reverses long-term HFHFD-induced metabolic disorders, lipid peroxidation, and ferroptosis

As NASH progression is accompanied by excessive oxidative stress[54,55], the present study examined hepatic ferroptosis biomarkers in mice fed a HFHFD for different durations (Supporting Information Fig. S1). As NASH progressed, the *Acsl4* proferroptotic gene was activated, but the *Gpx4* antiferroptotic gene was inhibited at the protein and mRNA levels (Supporting Information Fig. S2). These data indicated that ferroptosis is a key event associated with NASH progression.

The protective effects of *A. muc* on metabolic disorders were subsequently investigated in HFHFD-fed mice. As expected, *A. muc* attenuated weight gain and relieved the abnormal ALT and AST levels induced by the HFHFD (Supporting Information Fig. S3A and S3B). Additionally, TC levels, the NAS, and hepatic lipid accumulation were ameliorated upon *A. muc* intervention, whereas serum triglyceride (TG) levels remained unchanged (Fig. S3C−S3G). Furthermore, *A. muc* normalized HFHFD-induced impaired insulin sensitivity, as shown by the IGTTs and fasting insulin levels (Fig. S3H and S3I).

Notably, we found *A. muc* reversed the accumulation of reactive oxygen species (ROS) in the liver and intestine of HFHFD-fed mice (Fig. 1A−C, and D). Alterations in hepatic pro- and antioxidative gene expressions, as well as lipid peroxidation indicators (MDA and the GSH−to−GSSG ratio), were in line with the pathological phenotypes (Fig. 1B−E, and F). Subsequent GO analysis *via* liver transcriptomics revealed that the oxidoreductase activity pathway was upregulated upon *A. muc* treatment, and gene set enrichment analysis (GSEA) also revealed that *A. muc* increased antioxidative and antiferroptotic abilities (Fig. 1G and H). Furthermore, *A. muc* significantly alleviated HFHFD-induced hepatic iron accumulation (Fig. 1I) and normalized the expressions of the *Acsl4* and *Gpx4* ferroptosis genes (Fig. 1J).

Because lipid peroxidation is a precursor of ferroptosis[8], hepatic lipid profile alterations upon *A. muc* intervention were examined *via* untargeted lipidomic analyses. There were significant differences in lipid composition among the groups (Supporting Information Fig. S4A), and *A. muc* treatment reversed HFHFD-induced elevations in TG abundance and normalized phosphatidylcholine (PC) enrichment (Fig. 2A and B). Further KEGG enrichment analyses revealed increased metabolism of glycerophospholipids (GPs), linoleic acid (LA), α-LA, and arachidonic acid (ARA) upon *A. muc* intervention (Fig. 2C). We thus checked free fatty acid (FA) profiles and found that proinflammatory ω-6 polyunsaturated fatty acids (PUFAs), especially ARA (C20:4) and adrenic acid (ADA; C22:4), were enriched in HFHFD-fed mice but reduced after *A. muc* treatment (Fig. 2D and E). PUFA-anchored PEs, specifically ARA-containing or ADA-containing PEs, are regarded as key phospholipids that undergo peroxidation, driving cells towards ferroptosis[56]. Consistently, the present data revealed that HFHFD increased the levels of ARA-PEs and key PE species, namely, PE 16:0_20:4 and PE 18:0_20:4 (Fig. 2F and Fig. S4B), whereas *A. muc* treatment reduced these levels. Moreover, the levels of other ARA-containing or ADA-containing GPs remained unchanged (Fig. S4C and S4D). We further checked genes involved in PUFA synthesis, and observed expressions of key gene *Fasn*, *Scd1*, *Fads1*, *Elovl4*, *Elovl7* and *Acsl4* were upregulated in HFHFD-fed mice, but reduced after *A. muc* treatment (Fig. 2G and H, Fig. S4E−S4H). Together, these data suggested that lipid peroxidation and ferroptosis participate in NASH progression, which can be reversed by *A. muc via* the inhibition of PUFA synthesis.

3.2. A. muc activates the hepatic AMPK/SIRT1/PGC-1α axis

AMPK acts as a primary sensor of mitochondrial stress, linking the energy state, redox conditions, and lipid metabolism[57]. Therefore, we tested whether *A. muc* treatment could activate

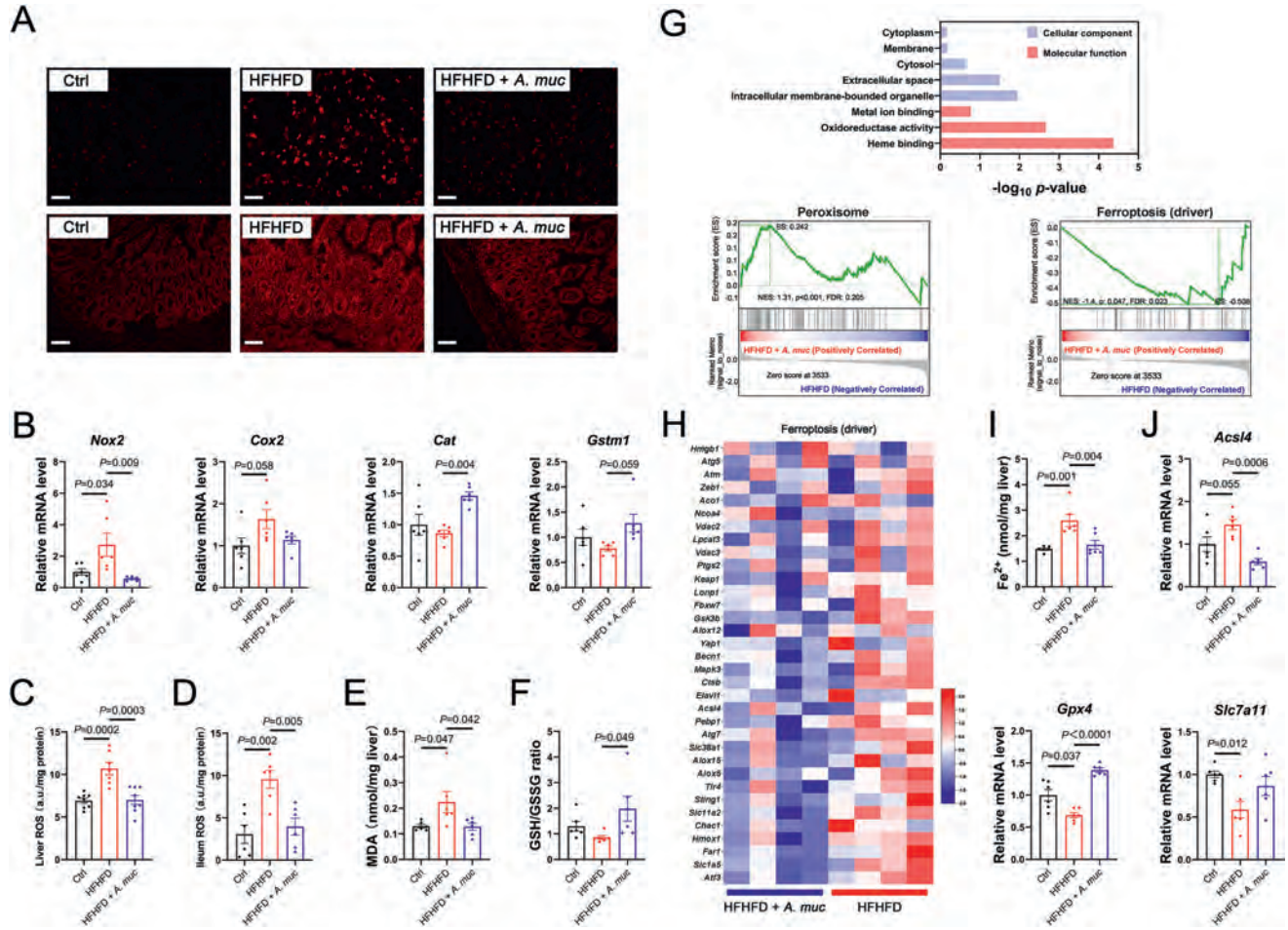

Figure 1 *A. muc* alleviates MAFLD-related hepatic lipid peroxidation and ferroptosis. (A) Representative DHE staining images of liver (upper channel, scale bar = 40 μm) and ileum (lower channel, scale bar = 20 μm) sections of HFHFD-fed mice treated with *A. muc* or vehicle. (B) mRNA expressions of hepatic oxidative genes analyzed by qPCR (normalized to GAPDH, n = 6/group). (C, D) Levels of ROS in the liver (C) and ileum (D) (n = 6/group). (E, F) Hepatic levels of MDA (E) and GSH to GSSG ratio (F) (n = 6/group). (G) Pathways up-regulated by *A. muc* based on unbiased GO analysis and GSEA plots of gene sets related with peroxisome and ferroptosis (n = 4/group). (H) Heatmap of gene expressions related with ferroptosis (n = 4/group). (I) Hepatic Fe^{2+} levels (n = 6/group). (J) mRNA expressions of ferroptotic genes analyzed by qPCR (normalized to GAPDH, n = 6/group). All data are presented as mean ± SEM.

AMPK in multiple tissues. As expected, *A. muc* intervention reversed the HFHFD-mediated decreases in AMPK activity in the liver, ileum, white adipose tissue (WAT), and brown adipose tissue (BAT), and this increase was strongest in the ileum (Fig. 3A). The expression of phosphorylated AMPK and ACC, as well as the expressions of the SIRT1 and PGC-1α downstream mediators, which are related to mitochondrial biogenesis[58], were also upregulated in response to *A. muc* stimulus (Fig. 3A–C). The relationship between AMPK activity and ferroptosis was further investigated. The expression of the AMPK downstream gene *Ppargc1a* (encoding PGC-1α) was negatively associated with the levels of the ferroptosis indicators MDA and Fe^{2+} (Fig. 3D). These results indicated that *A. muc* treatment could promote AMPK activity in the host, including the liver, which may contribute to protection against ferroptosis. Considering that *A. muc* colonizes in the intestine, we supposed *A. muc* may regulate hepatic AMPK activity *via* the production of specific microbiota-derived metabolites.

3.3. A. muc regulates intestinal and hepatic short-chain fatty acid (SCFA) metabolism

A previous study has demonstrated that *A. muc* exerts antioxidative effect on MAFLD by increasing L-aspartate (L-Asp) levels (28). Therefore, we examined L-Asp levels in the liver. L-Asp was depleted after HFHFD feeding, whereas no significant difference was observed with *A. muc* treatment (Fig. 4A), which indicated that other metabolites mediate the antiferroptotic effect of *A. muc*.

SCFAs are microbial products fermented from dietary fibres, among which acetic acid has been reported to activate enterocyte AMPK signals[36,59]. Therefore, SCFA quantification assays were conducted using the stool and liver samples. We observed *A. muc* treatment reversed the HFHFD-induced depletion of total SCFAs in the gut and liver (Fig. 4B). Acetic acid, propionic acid, and butyric acid, which constitute the vast majority of the SCFA pool, were significantly enriched due to *A. muc* supplementation (Fig. 4C and D). Consistently, SCFA receptors were upregulated in the ileum and

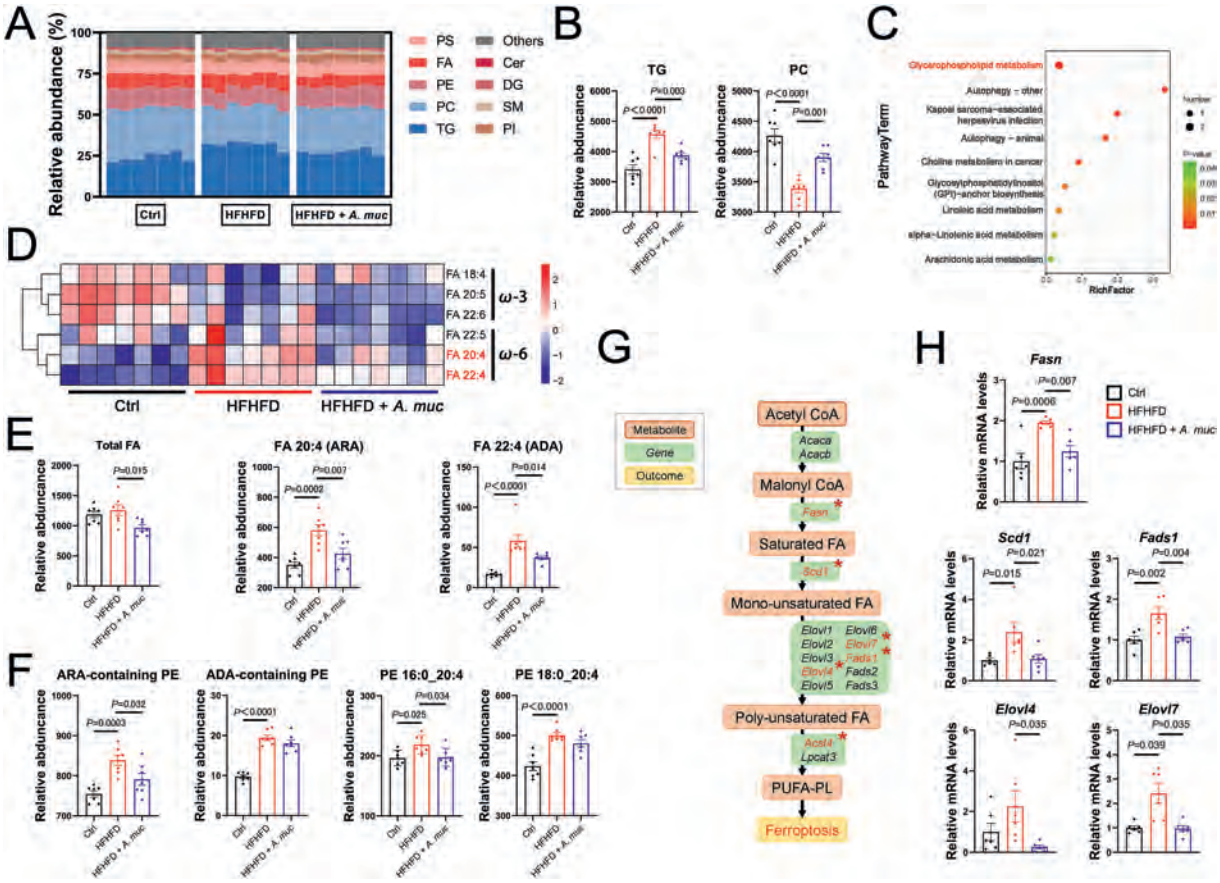

Figure 2 *A. muc* reshapes hepatic lipid spectrum and alleviated accumulation of ARA-containing PEs. (A, B) Lipid profiles (A) and relative abundances of TG and PC (n = 7/group) (B). (C) KEGG enrichment analysis based on hepatic lipidomics between the HFHFD-fed and *A. muc*-treated mice. (D, E) Heatmap diagram of free FAs (D) and relative abundance of total FA, ARA and ADA among groups (n = 7/group) (E). (F) Relative abundances of ARA-containing or ADA-containing PEs, PE 16:0_20:4 and PE 18:0_20:4 (n = 7/group). (G) PUFA synthesis diagram with related metabolites and genes. (H) Significant gene expressions related with PUFA synthesis upon *A. muc* intervention analyzed by qPCR (normalized to GAPDH, n = 6/group). All data are presented as mean ± SEM.

liver (Fig. 4E). Because the gut barrier is strongly associated with SCFA levels and NASH progression[60], we subsequently tested gut barrier function. *A. muc* elevated tight junction gene expressions and mucus layer thickness in HFHFD-fed mice (Fig. 4F and G), which was in line with previous studies[34,35]. Moreover, there was no difference in the mucus layer between the HFHFD-fed mice and control mice, which may be due to a host protective mechanism against SCFA depletion and intestinal oxidative stress[61].

AMPK is a complex regulated by several factors, including the AMP-to-ATP ratio, LKB1 expression, or Ca^{2+} level[62]. To investigate which factor is primarily involved, the hepatic concentrations of AMP and ATP were measured. We found the AMP-to-ATP ratio was significantly elevated upon *A. muc* treatment (Fig. 4H), whereas the expressions of Lkb1 and Camkk2 (receptor of Ca^{2+}) remained unchanged (Fig. 4I). These results indicated that microbiota-derived SCFAs may be key metabolites that participate in hepatic AMPK activation by increasing the AMP-to-ATP ratio during *A. muc* intervention.

3.4. Acetate activates hepatic AMPK signalling to defend against lipid peroxidation

AMPK can be activated by mild perturbations in ATP synthesis[57], which may explain why a HFHFD inhibits AMPK activity through excessive energy status. SCFAs are correlated with AMPK activity[63], but the specific SCFAs that regulate hepatic AMPK are unclear. Therefore, the present study investigated the effects of three primary SCFA types in the human and mouse SCFA pools on AMPK activity and their antiferroptotic ability. No differences in food intake were detected upon SCFA treatments (Supporting Information Fig. S5A). In addition, acetate and butyrate activated the hepatic AMPK/SIRT1/PGC-1α axis in HFHFD-fed mice, while acetate activated this axis to a greater extent (Fig. 5A–C and Fig. S5B). The AMP to ATP ratio was elevated after acetate treatment (Fig. 5D). Similarly, only the mice treated with acetate presented reduced levels of lipid peroxidation and

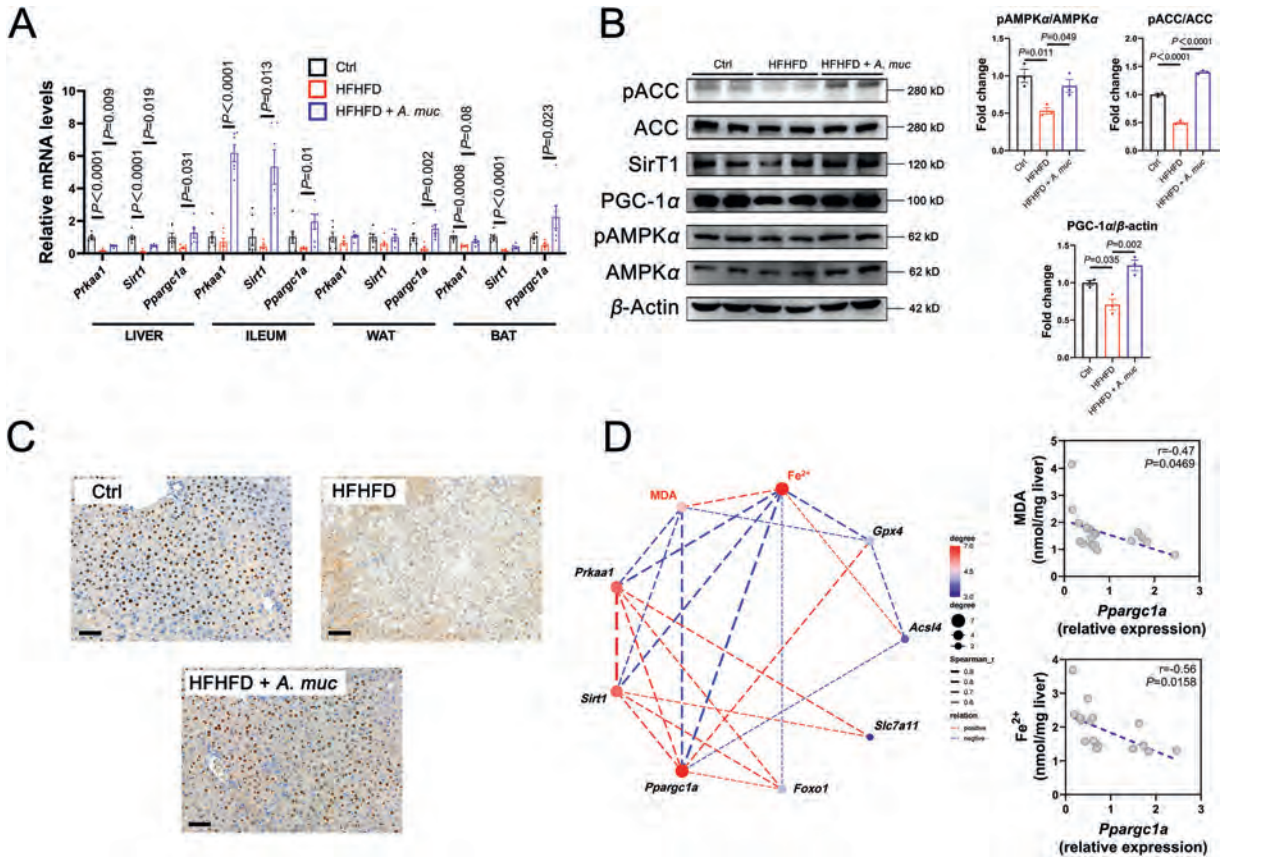

Figure 3 *A. muc* activates hepatic AMPK/SIRT1/PGC-1α signaling. (A) mRNA expressions of AMPK genes in different tissues analyzed by qPCR (normalized to GAPDH, $n = 6$/group). (B) Liver expressions of AMPK genes analyzed by Western blot ($n = 2$/group) and protein expressions of the phosphorylated AMPKα, phosphorylated ACC and PGC-1α in the indicated groups (normalized to AMPKα, ACC and β-actin, respectively, $n = 3$/group). (C) Representative images of liver sections with PGC-1α immunohistochemistry staining, scale bar = 20 μm. (D) Correlations among levels of ferroptosis biomarkers and hepatic expressions of AMPK genes and ferroptosis genes. All data are presented as mean ± SEM.

ferroptosis (Fig. 5E−G, Supporting Information Figs. S6 and S5B), whereas these SCFAs downregulated the expression of *Srebp-1c*, the main regulator of lipid synthesis (Fig. 5G). Consistent with the *in vivo* results, the *in vitro* model also indicated that acetate rescued the AMPK activity inhibited by erastin and protected AML12 and HepG2 cells from lipid peroxidation and ferroptosis (Fig. 5H−J and Fig. S5C−S5F). These data identified microbiota-derived acetate as the primary hepatic AMPK activator that defends against lipid peroxidation and ferroptosis.

3.5. A. muc exerts antiferroptotic effects via the activation of AMP synthesis

The intestinal microbiota consists of many SCFA-producing microbes. To elucidate the unique antiferroptotic impact of *A. muc*, HFHFD-fed mice were treated with several typical SCFA-producing microbes (*B. longum*, *E. coli*, and *L. reuteri*). Notably, only the mice treated with *A. muc* presented decreased MDA levels and normalized expressions of ferroptosis-related genes (Fig. 6A and B). Quantification of SCFA levels in the liver demonstrated that only *A. muc* treatment enriched acetic acid and activated the hepatic AMPK/SIRT1/PGC-1α axis (Fig. 6C and D). Consistently, hepatic AMPK activation and an elevated AMP-to-ATP ratio were observed only in mice treated with *A. muc* (Fig. 6E), suggesting that the antiferroptotic effect of *A. muc* on MAFLD is related to AMP-triggered AMPK activation.

Acetate is converted into AMP and acetyl-CoA *via* acyl-CoA synthetase short-chain family member 1 (ACSS1) and ACSS2 in mitochondria[64,65]. Because *A. muc* significantly enriches AMP in the liver, we hypothesized that *A. muc* may regulate the transformation of acetate and the synthesis of AMP. Consistent with our hypothesis, the by-product acetyl-CoA was enriched (Fig. 6F), and the expression of key gene *Acss1* was upregulated upon *A. muc* treatment (Fig. 6G). These data suggested that *A. muc* may upregulate Acss1 to promote AMP synthesis, further triggering AMPK activation to defend against lipid peroxidation.

3.6. AMPK activation is crucial to the antiferroptotic effect of A. muc

To elucidate whether AMPK activation is necessary for the antiferroptotic effect of *A. muc*, hepatic-targeted adeno-associated virus (AAV)-shRNA was utilized to specifically knockdown hepatic *Prkaa1* in *A. muc*-treated mice. AAV-shPrkaa1 injection significantly inhibited the AMPK/SIRT1/PGC-1α axis (Fig. 7A−C and Supporting Information Fig. S7A). Moreover, knockdown of hepatic *Prkaa1* significantly abolished the antiferroptotic effect of *A. muc*, which was characterized by elevated *Acsl4*

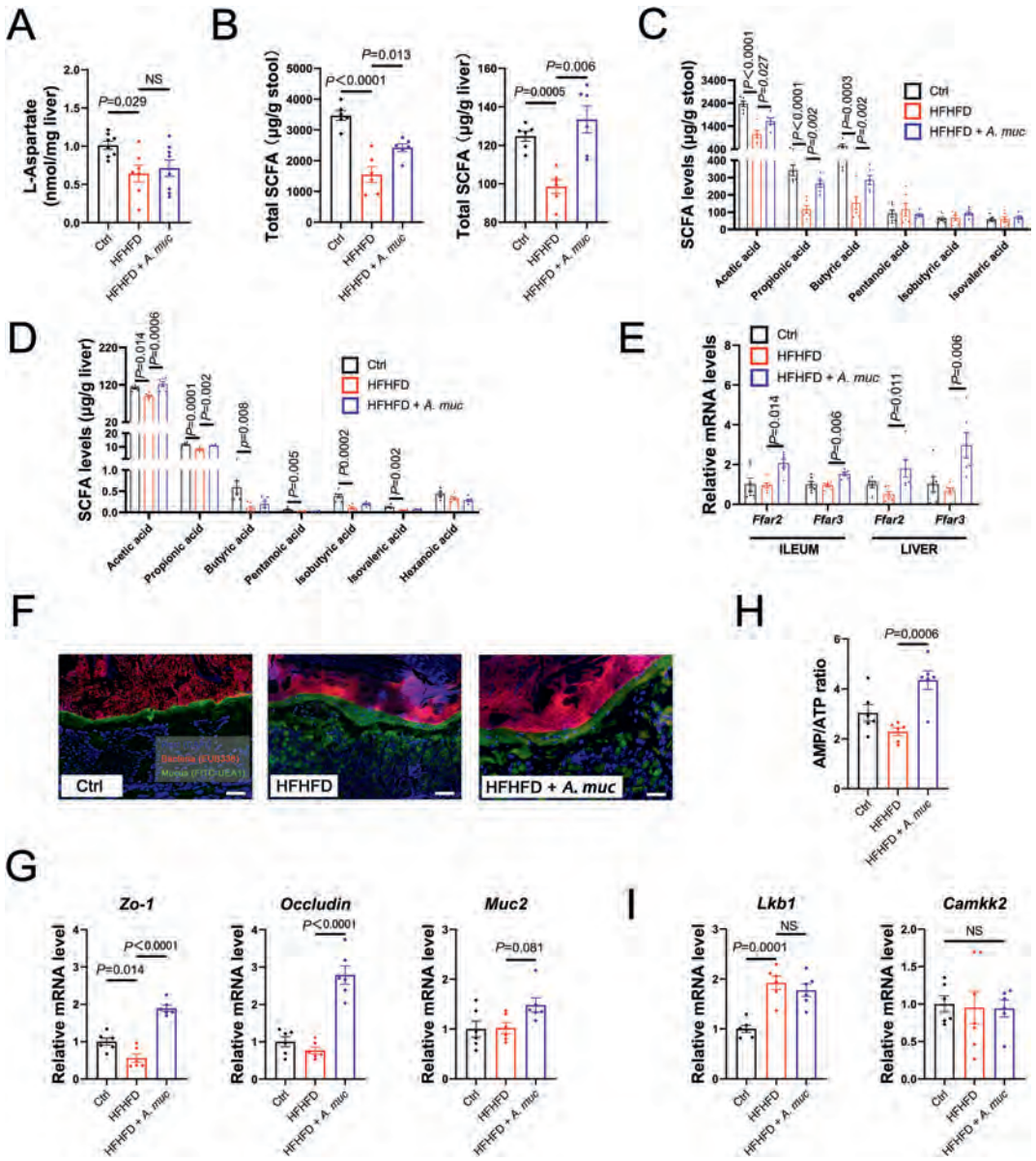

Figure 4 *A. muc* regulates short chain fatty acid metabolism and strengthened gut barrier integrity. (A) Hepatic L-aspartate concentrations. (B) Total SCFA levels in the stool and liver samples (n = 6/group). (C, D) SCFA profiles in the stool (C) and liver (D) samples (n = 6/group). (E) mRNA expressions of SCFA receptor genes (normalized to GAPDH, n = 6/group). (F) Representative images of pellet-containing distal colon sections stained with DAPI (blue), FITC-UEA1 (green) and bacteria EUB338 probe (red), scale bar = 40 μm. (G) mRNA expressions of gut barrier protective genes (normalized to GAPDH, n = 6/group). (H) Hepatic AMP to ATP ratio (n = 6/group). (I) mRNA expressions of AMPK regulator *Lkb2* and *Camkk2* (normalized to GAPDH, n = 6/group). All data are presented as mean ± SEM. NS, no significant difference.

expression, as well as decreased *Gpx4* expression (Fig. 7D) and lipid peroxidation levels (Fig. 7E–G and Fig. S7B). Furthermore, Compound C (CC), an AMPK inhibitor, was used in the *in vitro* model to knockdown AMPK expression (Fig. 7H, Fig. S7C and S7D). The antiferroptotic effect of acetate was abrogated when the cells were exposed to CC (Fig. 7I and J, Fig. S7E and S7F). These results highlighted that hepatic AMPK activation is crucial to the ability of *A. muc* to prevent lipid peroxidation and ferroptosis.

3.7. A. muc-mediated AMPK activation and the protective effect against lipid peroxidation are independent of the gut microbiota

A. muc regulates SCFA metabolism by direct fermentation or cross-feeding with SCFA-producing microbes[66,67]. To reveal the role of the gut microbiota in *A. muc*-mediated AMPK activation, the faecal microbiota was transferred from HFHFD-fed and *A. muc*-treated mice to new HFHFD-fed mice. Transmissible phenotypes, characterized by downregulation of *Ppargc1a*

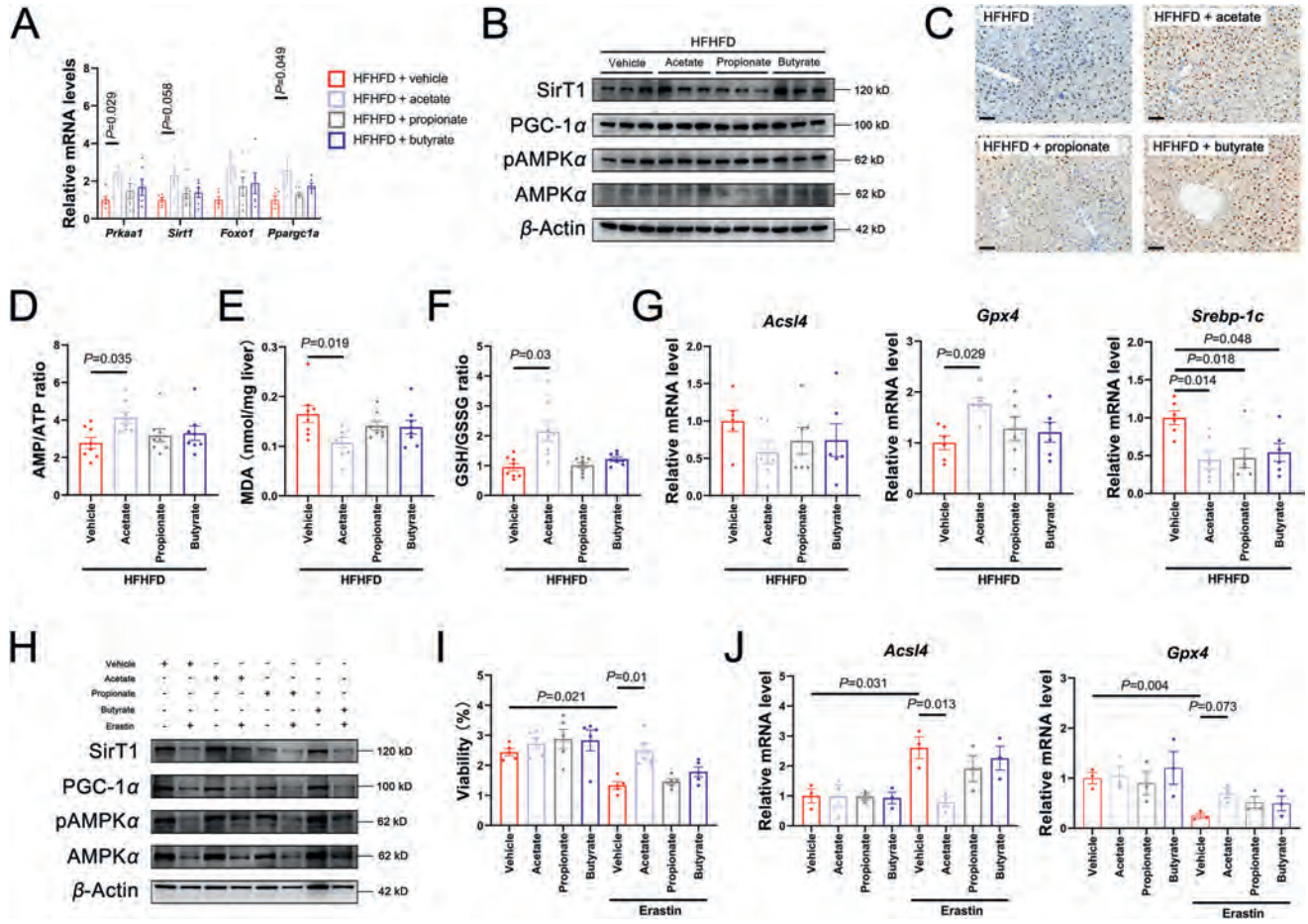

Figure 5 Acetate activates hepatic AMPK signaling. (A, B) Hepatic AMPK gene expressions of HFHFD-fed mice tread with SCFAs analyzed by qPCR (normalized to GAPDH, $n = 6$/group) (A) and Western blot ($n = 3$/group) (B). (C) Representative images of liver sections with PGC-1α immunohistochemistry staining, scale bar = 20 μm. (D) Hepatic AMP to ATP ratio ($n = 8$/group). (E, F) Hepatic levels of MDA (E) and GSH to GSSG ratio (F) ($n = 6$/group). (G) mRNA expressions of ferroptotic genes analyzed by qPCR (normalized to GAPDH, $n = 6$/group). (H) Liver expressions of AMPK genes of the human hepatocellular carcinoma cell line HepG2 treated with SCFAs in the presence or absence of 2 μmol/L erastin challenge analyzed by Western blot (normalized to GAPDH, $n = 1$/group). (I) Viability detected by CCK-8 assay in the human hepatocyte line AML12 treated with SCFAs with or without 2 μmol/L erastin ($n = 5$/group). (J) mRNA expressions of ferroptotic genes analyzed by qPCR (normalized to GAPDH, $n = 3$/group). All data are presented as mean ± SEM.

expressions and GSH concentrations but elevated ROS and MDA levels, were observed in mice receiving the HFHFD-derived microbiota, and an opposite trend was observed in mice receiving the *A. muc*-derived microbiota (Fig. 8A−D). 16S rRNA sequencing revealed enrichments of the SCFA producers Ruminococcaceae and *Roseburia* in the *A. muc*-derived microbiota (Supporting Information Fig. S8A). To further investigate the impact of *A. muc* on SCFA metabolism, we colonized germ-free mice with *A. muc*, and fed them with HFHFD for up to 8 weeks. *A. muc* colonization rescued the HFHFD-induced reduction in total SCFAs in the liver (Fig. 8E). Moreover, *A. muc* increased the hepatic levels of acetic acid and propionic acid but not butyric acid (Fig. 8F). Furthermore, AMPK/SIRT1/PGC-1α signalling was activated due to *A. muc* colonization (Fig. 8G and H). Mice colonized with *A. muc* exhibited relieved ROS overload (Fig. 8I) and ameliorated hepatic ferroptotic markers (Fig. 8J and K, Fig. S8B). These data suggested that an *A. muc*-dominated microbiota or *A. muc* itself mediates protective effects against lipid peroxidation. Additionally, *A. muc* may increase butyric acid levels by crossfeeding with other butyric acid-producing microbes, but *A. muc* rarely produces butyric acid. Thus, *A. muc*-derived acetate mediated, at least partially, its antiferroptotic effect on NASH by activating hepatic AMPK activity.

4. Discussion

Because *A. muc* has been shown to exert antioxidative effects in previous studies[30-32], the present study further investigated the antiferroptotic effects of *A. muc* on MAFLD and the underlying molecular mechanism. The present study identified acetate as a key *A. muc*-derived metabolite that activates hepatic AMPK signalling to ameliorate lipid peroxidation and ferroptosis.

Iron overload is widely acknowledged to be common in patients with MAFLD, and iron-induced lipid peroxidation and insulin resistance are typical characteristics of MAFLD[68,69]. Consistent with previous studies, we confirmed the accumulation of hepatic ROS, iron, and lipid peroxides in MAFLD mice. *A. muc* alleviated the peroxidation state in the liver and normalized

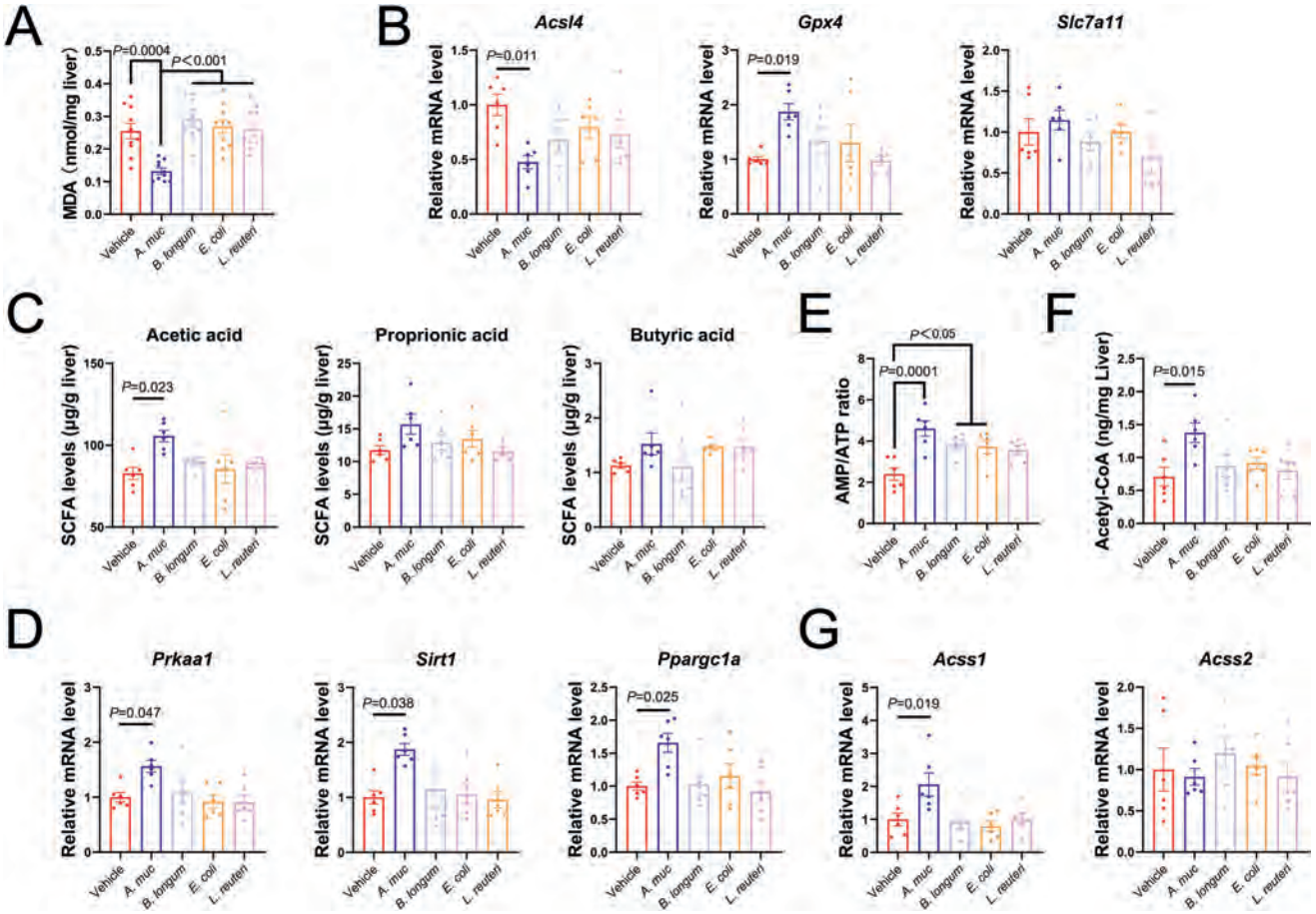

Figure 6 *A. muc* upregulates AMP synthesis to activate AMPK signaling and alleviate ferroptosis. (A) Hepatic levels of MDA in HFHFD-fed mice treated with several SCFA-producing microbes (n = 10/group). (B) Hepatic ferroptosis gene expressions analyzed by qPCR (normalized to GAPDH, n = 6/group). (C) Hepatic SCFA concentrations (n = 6/group). (D) Hepatic AMPK gene expressions analyzed by qPCR (normalized to GAPDH, n = 6/group). (E, F) Hepatic AMP to ATP ratio (n = 6/group) (E) and acetyl-CoA levels (n = 6/group) (F). (G) Hepatic mRNA levels of gene involved in AMP synthesis were analyzed by qPCR (normalized to GAPDH, n = 6/group). All data are presented as mean ± SEM.

abnormal peroxide accumulation and transaminase (ALT, AST) levels. The hepatic lipidomic results indicated that free ARA and ARA-PEs were enriched with HFHFD-feeding but reduced after *A. muc* treatment. ARA-anchored PEs are key mediators of ferroptosis, which could be peroxided under oxidative stimuli, subsequently impairing the cell membrane to trigger ferroptosis[70,71]. Therefore, we further investigated genes involved in PUFA synthesis. Notably, we identified several key targeted genes regulated by *A. muc*. *Fasn* and *Scd1* function in the synthesis of saturated FAs (SFAs) and monounsaturated FAs (MUFAs), respectively[72]. *Elovl4*, *Elovl7,* and *Fads1* are essential for the elongation of FAs[73,74]. *Acsl4* is the key proferroptotic gene responsible for anchoring PUFAs in glycerol phospholipids in the cell membrane[75]. These data indicated that *A. muc* partially alleviates MAFLD-related ferroptosis *via* the inhibition of PUFA synthesis.

Accumulating evidence has linked energy metabolism with redox states and ferroptosis[76-78]. Because *A. muc* regulates metabolic processes, we hypothesized that the antiferroptotic effect of *A. muc* may be related to metabolic alterations. In line with the latest studies showing that *A. muc* regulates AMPK activity[30,79], the present study verified that *A. muc* activated the AMPK pathway in the majority of tissues expressing AMPK, including the liver, ileum, WAT, and BAT. The expression of the AMPK downstream genes *SIRT1* and *PGC-1α*, which are closely related to anti-inflammatory effects *via* the inhibition of NF-κB[80,81], was increased. *PGC-1α* is responsible for regulating mitochondrial biosynthesis, and it chelates iron and protects against Fenton reaction-induced lipid peroxidation[82]. Consistently, we found strong correlations between the expressions of *Ppargc1a* and ferroptotic genes. Therefore, we speculated that *A. muc* may exert its antiferroptotic effect by activating the AMPK/SIRT1/PGC-1α axis. Moreover, AMPK activation was the strongest in the ileum, the target where *A. muc* colonizes, which may be due to the enrichment of *A. muc*-derived metabolites.

SCFAs are primary gut commensal bacteria-derived metabolites that participate in the energy metabolism of colonocytes and hepatocytes[37]. SCFAs exert various beneficial effects on target tissues. For example, butyrate strengthens gut barrier integrity and increases mucus layer thickness[83], which may be mediated by intestinal AMPK activation[84], and we observed a similar trend in the present study. In the liver, acetate is a substrate used to synthesize cholesterol and fatty acids[85], whereas propionate is related to gluconeogenesis[86]. In the present study, SCFAs were enriched in the liver and intestine upon *A. muc* treatment, which was in line with the activation of AMPK and the upregulation of SCFA receptor gene expression of these two targets. These data provide additional clues to explain the AMPK-activating effects of SCFAs. A previous study has demonstrated that L-Asp mediates the

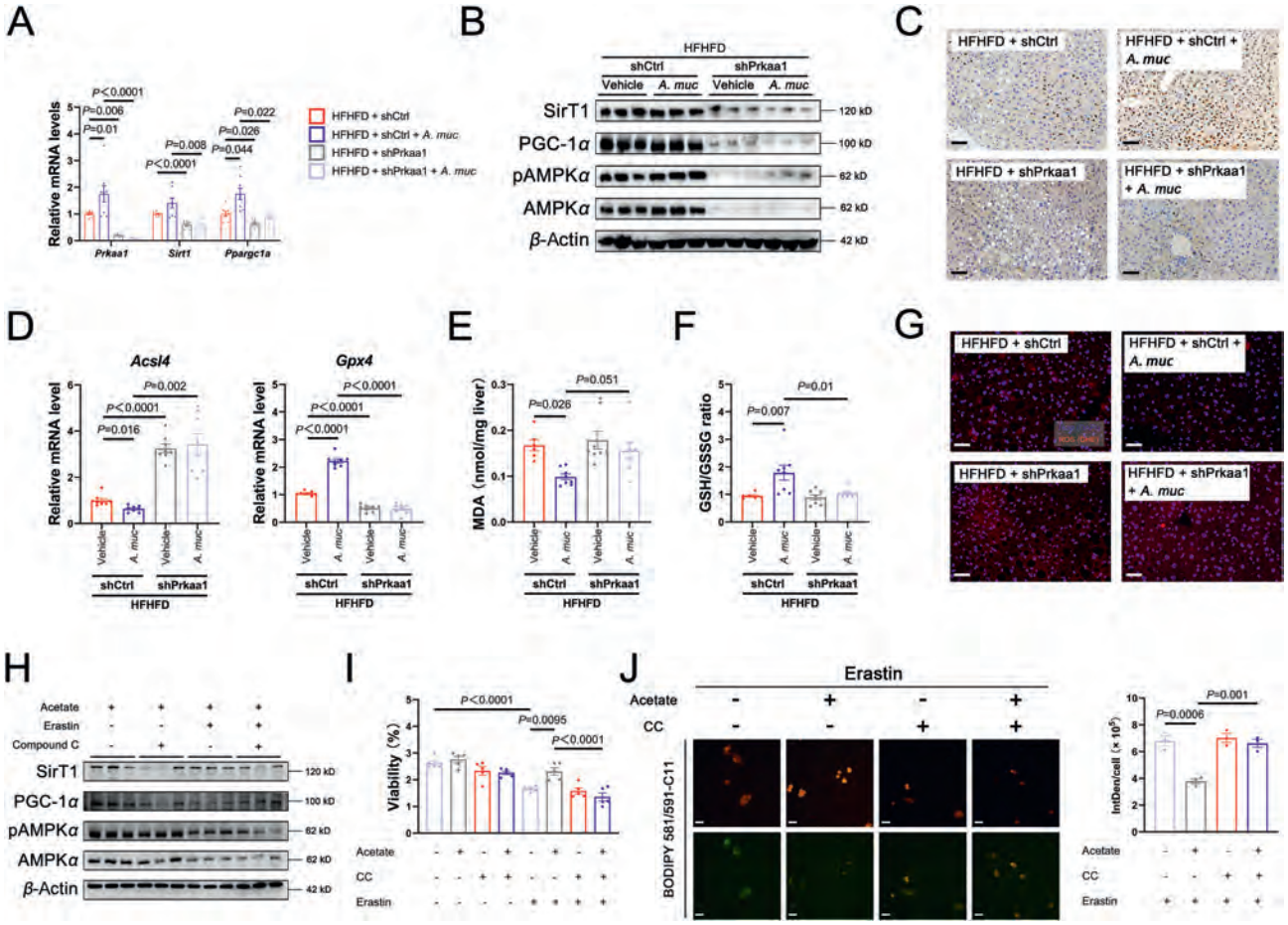

Figure 7 AMPK activation contributes to the protective effect of *A. muc* against lipid peroxidation. (A, B) Hepatic AMPK gene expressions of HFHFD-fed mice treated with *A. muc* with shPrkaa1 or ShCtrl analyzed by qPCR (normalized to GAPDH, $n = 6$/group) (A) and Western blot ($n = 3$/group) (B). (C) Representative images of liver sections with PGC-1α immunohistochemistry staining, scale bar = 20 μm. (D) mRNA expressions of ferroptotic genes analyzed by qPCR (normalized to GAPDH, $n = 6$/group). (E, F) Hepatic levels of MDA (E) and GSH to GSSG ratio (F) ($n = 6/8/8/8$). (G) Representative images of liver sections stained with DHE, scale bar = 40 μm. (H) Expressions of AMPK genes of the human hepatocellular carcinoma cell line HepG2 treated with sodium acetate in the presence or absence of 2 μmol/L Compound C and 2 μmol/L erastin challenge analyzed by Western blot ($n = 3$/group). (I) Viability detected by CCK-8 assay in the human hepatocyte line AML12 treated with sodium acetate in the presence or absence of 2 μmol/L Compound C and 2 μmol/L erastin challenge ($n = 5$/group). (J) Representative C11-BODIPY staining images and related quantification of HepG2 treated with 2 μmol/L erastin with or without 0.5 mmol/L acetate and 2 μmol/L Compound C, scale bar = 20 μm. All data are presented as mean ± SEM.

antioxidative effect of *A. muc* against MAFLD *via* the LKB1−AMPK-dependent pathway[30]. Thus, the hepatic L-Asp levels upon *A. muc* treatment were evaluated in the present study. There were no changes in hepatic L-Asp levels. We speculated that different diet compositions and different *A. muc* interventions may be responsible for these contradictory results.

Analysis of which SCFA activates AMPK in the liver suggested that acetate, but not propionate or butyrate, is the key activator of the hepatic AMPK pathway. Acetate is metabolized by enterocytes to acetyl-CoA and AMP, thereby activating the intestinal AMPK/PGC-1α/PPARα pathway to promote lipid oxidation in the colon[87]. Consistently, the present findings indicated that *A. muc* treatment increases the hepatic AMP-to-ATP ratio, which is regarded as the main activator of AMPK, thus explaining the molecular mechanism by which acetate activates hepatic AMPK.

Acetate is the most abundant SCFA in humans, with an average concentration of 260 μmol/L, compared with 30 μmol/L each for propionate and butyrate[38]. The present study demonstrated that the highest levels of acetate were in the stool and liver, suggesting that acetate may mediate most of the effects of SCFAs. A recent study has revealed that acetate ameliorates lipid metabolism and insulin resistance in MAFLD by activating the hepatic FFAR2 pathway[39]. On the basis of these findings, we additionally verified that acetate mediates antioxidative effects against lipid peroxidation in MAFLD and in an *in vitro* erastin challenge. Interestingly, we found that all three SCFAs downregulated the expression of *Srebp-1c*, a key mediator of liver lipid synthesis. These findings suggested that the antiferroptotic effect of acetate is related to AMPK activation and that the *A. muc*-mediated anti-ferroptotic effect occurs, at least partially, through the enrichment of acetate in the liver.

Considering the unique antiferroptotic effect of acetate, we proposed whether other SCFA-producing microbes could exert this effect. However, only *A. muc* effectively alleviated lipid peroxidation and ferroptosis. In addition, only *A. muc* enriched acetic acid in the liver and further activated the AMPK/SIRT1/

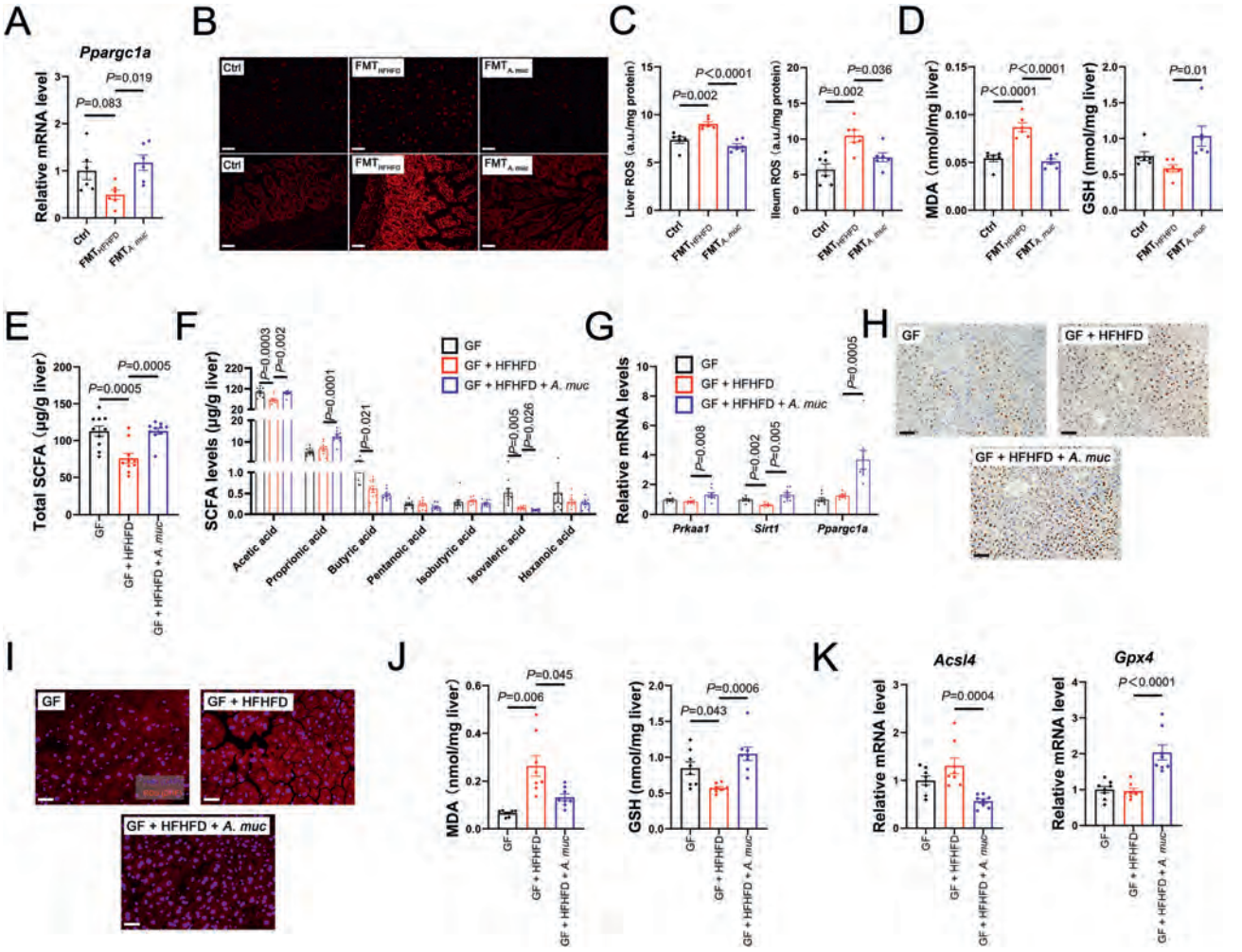

Figure 8 *A. muc*-mediated protective effect against lipid peroxidation is independent of the gut microbiota. (A) Hepatic *Ppargc1a* expression of the FMT recipient mice. (B) Representative DHE staining images of liver (upper channel, scale bar = 40 μm) and ileum (lower channel, scale bar = 20 μm) sections. (C) Levels of ROS in the liver and ileum (n = 6/group). (D) Hepatic levels of MDA and GSH (n = 6/group). (E, F) Total SCFA levels (E) and profiles (F) in the liver (n = 10/group). (G) AMPK gene expressions were analyzed by qPCR (normalized to GAPDH, n = 8/group). (H) Representative images of liver sections with PGC-1α immunohistochemistry staining of HFHFD-fed germ-free mice treated with *A. muc* or vehicle, scale bar = 20 μm. (I) Representative images of liver sections with DHE staining, scale bar = 40 μm. (J) Hepatic levels of MDA and GSH (n = 8/group). (K) mRNA expressions of ferroptotic genes and oxidative genes (normalized to GAPDH, n = 8/group). All data are presented as mean ± SEM.

PGC-1α pathway, which is associated with AMP synthesis. These results may explain why *A. muc* inhibits ferroptosis, whereas other SCFA-producing microbes cannot. Mechanistically, *A. muc* upregulates *Acss1* expression to promote AMP synthesis, which further activates AMPK signalling, thereby exerting its anti-ferroptotic effect.

The role of AMPK activation in ferroptosis remains controversial[88]. The present study further revealed that AMPK activation is essential for *A. muc*- or acetate-mediated antiferroptotic effects, as demonstrated by the deficiency of hepatic *prkaa1* leading to reductions in antioxidative ability and elevations in lipid peroxidation markers, both *in vivo* and *in vitro*. Additionally, erastin-induced ferroptosis inhibited AMPK activity, suggesting that hepatocellular AMPK activity is associated with the ferroptotic state. Moreover, the present data confirmed that the AMPK downstream genes SIRT1 and PGC-1α mediate the anti-ferroptotic effect, which is inconsistent with previous studies, indicating that AMPK-mediated ACC phosphorylation inhibits ferroptosis[89] or that BECN1 phosphorylation promotes ferroptosis[90]. There are several differences between the present study and previous studies. First, the latter study indicated that AMPK-mediated BECN1 phosphorylation inhibits *SLC7A11*-mediated cystine transport to promote ferroptosis, and the present study demonstrated that *SLC7A11* expression was not significantly altered upon AMPK activation by *A. muc* or AMPK deficiency by AAV-shRNA and CC (Fig. 1J, Supporting Information Figs. S5B and S9). We supposed that AMPK primarily regulates PUFA synthesis and GSH levels to modulate ferroptosis *via* the inhibition of ACSL4 and the activation of GPX4. Second, previous results have been based on cancer cell lines induced by erastin or glucose starvation, whereas the present study adopted a murine MAFLD model with more complicated ferroptotic factors. Furthermore, compared with those in previous cell experiments, the host microbiota and microbiota-derived metabolites were involved in the present study. These

discrepancies suggest that the AMPK-mediated regulation of ferroptosis may be dependent on the metabolic environment and the gut microbiota, thereby requiring further investigation.

Contradictory results have been reported between human and mouse subjects regarding whether *A. muc* intervention could induce alterations in the gut microbiota[25,31,34,35]. Therefore, the present study investigated whether *A. muc*-mediated beneficial effects are self-generated or result from the regulation of the gut microbiota. The present findings confirmed that *A. muc*-mediated AMPK activation was independent of the gut microbiota. In addition, transmissible phenotypes were observed *via* faecal microbiota transplantation, suggesting that gut microbes mediate these alterations. However, colonization of germ-free mice with *A. muc* showed a similar alleviation of ferroptosis independent of the gut microbiota, indicating that *A. muc* itself exerts an anti-ferroptotic effect rather than by enriching other microbes. Additionally, the colonization of *A. muc* enriched acetic acid and propionic acid, but not butyric acid, in the liver. This finding indicated that *A. muc* itself seldom produces butyrate. Then, we subsequently verified that *A. muc* was enriched with butyrate-producing *Ruminococcaceae* and *Roseburia* in wild-type mice[91,92]. Thus, the elevation of butyrate levels in *A. muc*-treated wild-type mice may result from crossfeeding with other butyrate-producing microbes[93].

A recent randomized controlled trial has revealed that daily oral supplementation of 10^{10} CFU *A. muc* is safe and well tolerated by human subjects[25]. The present study demonstrated that *A. muc* is a biocompatible and beneficial probiotic for treating lipid peroxidation in MAFLD. However, our study had several limitations. First, our study revealed that *A. muc* activated AMPK activity in a few tissues, including the ileum, where acetate is the most abundant. Thus, whether acetate inhibits intestinal ferroptosis through ileal AMPK activation requires further investigation. Additionally, we found that *A. muc* decreased the accumulation of hepatic peroxides, especially ARA-containing PEs. However, specific lipid effectors should be identified and verified to better understand the role of ferroptosis in MAFLD progression. Previous studies have revealed the contradictory effects of ferroptosis on the progression or regression of liver fibrosis. By targeting hepatocytes, ferroptosis triggers chronic liver injury and fibrosis[94,95], whereas ferroptosis of HSCs has been adopted as a therapeutic approach for treating fibrosis[96,97]. Thus, future studies should address the role of *A. muc* and *A. muc*-derived acetate in MAFLD-related fibrosis.

5. Conclusions

The present study highlights another new mechanism by which the probiotic *A. muc* ameliorates MAFLD *via* inhibiting lipid peroxidation and ferroptosis. Mechanistically, the *A. muc*-derived metabolite acetate is transported and metabolized to AMP in the liver, activating the hepatic AMPK/SIRT1/PGC-1α axis to protect against PUFA synthesis, which is mediated by *A. muc* itself independent of the gut microbiota.

Data availability

The 16S rRNA sequencing and liver RNA-seq datasets were uploaded to the Sequence Read Archive (SRA) database under BioProject numbers PRJNA884086 and PRJNA884314, respectively.

Acknowledgments

This study was supported by the National Natural Science Foundation of China (81790631, 81874142, and 82073041), the National Key Research and Development Program of China (2018YFC2000500, 2021YFA1301104, and 2021YFC2301804), the CAMS Innovation Fund for Medical Sciences (2019-I2M-5-045, China), the Research Project of Jinan Microecological Biomedicine Shandong Laboratory (JNL-2022001A, China), and the China Postdoctoral Science Foundation (2023M743125).

Author contributions

Aoxiang Zhuge: Writing − review & editing, Writing − original draft, Validation, Investigation, Funding acquisition, Formal analysis, Data curation, Conceptualization. Shengjie Li: Investigation, Formal analysis, Data curation, Conceptualization. Shengyi Han: Investigation, Data curation. Yin Yuan: Investigation, Data curation. Jian Shen: Investigation. Wenrui Wu: Investigation. Kaicen Wang: Validation. Jiafeng Xia: Validation. Qiangqiang Wang: Software, Resources. Yifeng Gu: Resources. Enguo Chen: Supervision, Conceptualization. Lanjuan Li: Visualization, Funding acquisition, Conceptualization.

Conflicts of interest

The authors declare that they have no conflicts of interest.

Appendix A. Supporting information

Supporting information to this article can be found online at https://doi.org/10.1016/j.apsb.2024.10.010.

References

1. Loomba R, Friedman SL, Shulman GI. Mechanisms and disease consequences of nonalcoholic fatty liver disease. *Cell* 2021;**184**:2537−64.
2. Yang RX, Zou ZS, Zhong BH, Deng H, He FP, Shi JP, et al. The pathologic relevance of metabolic criteria in patients with biopsy-proven nonalcoholic fatty liver disease and metabolic dysfunction associated fatty liver disease: a multicenter cross-sectional study in China. *Hepatobiliary Pancreat Dis Int* 2021;**20**:426−32.
3. Huby T, Gautier EL. Immune cell-mediated features of non-alcoholic steatohepatitis. *Nat Rev Immunol* 2022;**22**:429−43.
4. Luedde T, Kaplowitz N, Schwabe RF. Cell death and cell death responses in liver disease: mechanisms and clinical relevance. *Gastroenterology* 2014;**147:**765-83.e4.
5. Schwabe RF, Tabas I, Pajvani UB. Mechanisms of fibrosis development in nonalcoholic steatohepatitis. *Gastroenterology* 2020;**158**:1913−28.
6. Fang X, Ardehali H, Min J, Wang F. The molecular and metabolic landscape of iron and ferroptosis in cardiovascular disease. *Nat Rev Cardiol* 2023;**20**:7−23.
7. Gautheron J, Gores GJ, Rodrigues CM. Lytic cell death in metabolic liver disease. *J Hepatol* 2020;**73**:394−408.
8. Stockwell BR. Ferroptosis turns 10: emerging mechanisms, physiological functions, and therapeutic applications. *Cell* 2022;**185**:2401−21.
9. Tong J, Li D, Meng H, Sun D, Lan X, Ni M, et al. Targeting a novel inducible GPX4 alternative isoform to alleviate ferroptosis and treat metabolic-associated fatty liver disease. *Acta Pharm Sin B* 2022;**12**:3650−66.

10. Luo P, Liu D, Zhang Q, Yang F, Wong YK, Xia F, et al. Celastrol induces ferroptosis in activated HSCs to ameliorate hepatic fibrosis *via* targeting peroxiredoxins and HO-1. *Acta Pharm Sin B* 2022;**12**: 2300−14.
11. Loguercio C, De Girolamo V, de Sio I, Tuccillo C, Ascione A, Baldi F, et al. Non-alcoholic fatty liver disease in an area of southern Italy: main clinical, histological, and pathophysiological aspects. *J Hepatol* 2001;**35**:568−74.
12. Nelson JE, Wilson L, Brunt EM, Yeh MM, Kleiner DE, Unalp-Arida A, et al. Relationship between the pattern of hepatic iron deposition and histological severity in nonalcoholic fatty liver disease. *Hepatology* 2011;**53**:448−57.
13. Sanyal AJ, Chalasani N, Kowdley KV, McCullough A, Diehl AM, Bass NM, et al. Pioglitazone, vitamin E, or placebo for nonalcoholic steatohepatitis. *N Engl J Med* 2010;**362**:1675−85.
14. Tsurusaki S, Tsuchiya Y, Koumura T, Nakasone M, Sakamoto T, Matsuoka M, et al. Hepatic ferroptosis plays an important role as the trigger for initiating inflammation in nonalcoholic steatohepatitis. *Cell Death Dis* 2019;**10**:449.
15. Musso G, Cassader M, Rosina F, Gambino R. Impact of current treatments on liver disease, glucose metabolism and cardiovascular risk in non-alcoholic fatty liver disease (NAFLD): a systematic review and meta-analysis of randomised trials. *Diabetologia* 2012;**55**: 885−904.
16. Qin N, Yang F, Li A, Prifti E, Chen Y, Shao L, et al. Alterations of the human gut microbiome in liver cirrhosis. *Nature* 2014;**513**:59−64.
17. Zhu L, Baker SS, Gill C, Liu W, Alkhouri R, Baker RD, et al. Characterization of gut microbiomes in nonalcoholic steatohepatitis (NASH) patients: a connection between endogenous alcohol and NASH. *Hepatology* 2013;**57**:601−9.
18. Aron-Wisnewsky J, Vigliotti C, Witjes J, Le P, Holleboom AG, Verheij J, et al. Gut microbiota and human NAFLD: disentangling microbial signatures from metabolic disorders. *Nat Rev Gastroenterol Hepatol* 2020;**17**:279−97.
19. Dong TS, Katzka W, Lagishetty V, Luu K, Hauer M, Pisegna J, et al. A microbial signature identifies advanced fibrosis in patients with chronic liver disease mainly due to NAFLD. *Sci Rep* 2020;**10**:2771.
20. Oh TG, Kim SM, Caussy C, Fu T, Guo J, Bassirian S, et al. A universal gut-microbiome-derived signature predicts cirrhosis. *Cell Metab* 2020;**32:**878-88.e6.
21. Sharpton SR, Schnabl B, Knight R, Loomba R. Current concepts, opportunities, and challenges of gut microbiome-based personalized medicine in nonalcoholic fatty liver disease. *Cell Metab* 2021;**33**: 21−32.
22. Chen ZR, Jin SF, Ma WB, Jiang RL. Intestinal microecology: a crucial strategy for targeted therapy of liver diseases. *Hepatobiliary Pancreat Dis Int* 2021;**20**:499−500.
23. Derrien M, Vaughan EE, Plugge CM, de Vos WM. *Akkermansia muciniphila* gen. Nov., sp. Nov., a human intestinal mucin-degrading bacterium. *Int J Syst Evol Microbiol* 2004;**54**:1469−76.
24. Everard A, Belzer C, Geurts L, Ouwerkerk JP, Druart C, Bindels LB, et al. Cross-talk between *Akkermansia muciniphila* and intestinal epithelium controls diet-induced obesity. *Proc Natl Acad Sci U S A* 2013;**110**:9066−71.
25. Depommier C, Everard A, Druart C, Plovier H, Van Hul M, Vieira-Silva S, et al. Supplementation with *Akkermansia muciniphila* in overweight and obese human volunteers: a proof-of-concept exploratory study. *Nat Med* 2019;**25**:1096−103.
26. Cani PD, Depommier C, Derrien M, Everard A, de Vos WM. *Akkermansia muciniphila*: paradigm for next-generation beneficial microorganisms. *Nat Rev Gastroenterol Hepatol* 2022;**19**:625−37.
27. Depommier C, Van Hul M, Everard A, Delzenne NM, De Vos WM, Cani PD. Pasteurized *Akkermansia muciniphila* increases whole-body energy expenditure and fecal energy excretion in diet-induced obese mice. *Gut Microbes* 2020;**11**:1231−45.
28. Routy B, Le Chatelier E, Derosa L, Duong CPM, Alou MT, Daillère R, et al. Gut microbiome influences efficacy of PD-1-based immunotherapy against epithelial tumors. *Science* 2018;**359**:91−7.
29. Schneider KM, Mohs A, Gui W, Galvez EJC, Candels LS, Hoenicke L, et al. Imbalanced gut microbiota fuels hepatocellular carcinoma development by shaping the hepatic inflammatory microenvironment. *Nat Commun* 2022;**13**:3964.
30. Rao Y, Kuang Z, Li C, Guo S, Xu Y, Zhao D, et al. Gut *Akkermansia muciniphila* ameliorates metabolic dysfunction-associated fatty liver disease by regulating the metabolism of L-aspartate *via* gut−liver axis. *Gut Microbes* 2021;**13**:1−19.
31. Xia J, Lv L, Liu B, Wang S, Zhang S, Wu Z, et al. *Akkermansia muciniphila* ameliorates acetaminophen-induced liver injury by regulating gut microbial composition and metabolism. *Microbiol Spectr* 2022;**10**:e0159621.
32. Cerro ED, Lambea M, Félix J, Salazar N, Gueimonde M, De la Fuente M. Daily ingestion of *Akkermansia mucciniphila* for one month promotes healthy aging and increases lifespan in old female mice. *Biogerontology* 2022;**23**:35−52.
33. Juárez-Fernández M, Porras D, Petrov P, Román-Sagüillo S, García-Mediavilla MV, Soluyanova P, et al. The synbiotic combination of *Akkermansia muciniphila* and quercetin ameliorates early obesity and NAFLD through gut microbiota reshaping and bile acid metabolism modulation. *Antioxidants (Basel)* 2021;**10**:2001.
34. Bian X, Wu W, Yang L, Lv L, Wang Q, Li Y, et al. Administration of *Akkermansia muciniphila* ameliorates dextran sulfate sodium-induced ulcerative colitis in mice. *Front Microbiol* 2019;**10**:2259.
35. Wu W, Lv L, Shi D, Ye J, Fang D, Guo F, et al. Protective effect of *Akkermansia muciniphila* against immune-mediated liver injury in a mouse model. *Front Microbiol* 2017;**8**:1804.
36. Dalile B, Van Oudenhove L, Vervliet B, Verbeke K. The role of short-chain fatty acids in microbiota−gut−brain communication. *Nat Rev Gastroenterol Hepatol* 2019;**16**:461−78.
37. Schönfeld P, Wojtczak L. Short- and medium-chain fatty acids in energy metabolism: the cellular perspective. *J Lipid Res* 2016;**57**:943−54.
38. Bloemen JG, Venema K, van de Poll MC, Olde Damink SW, Buurman WA, Dejong CH. Short chain fatty acids exchange across the gut and liver in humans measured at surgery. *Clin Nutr* 2009;**28**: 657−61.
39. Aoki R, Onuki M, Hattori K, Ito M, Yamada T, Kamikado K, et al. Commensal microbe-derived acetate suppresses NAFLD/NASH development *via* hepatic FFAR2 signalling in mice. *Microbiome* 2021;**9**:188.
40. Haghikia A, Zimmermann F, Schumann P, Jasina A, Roessler J, Schmidt D, et al. Propionate attenuates atherosclerosis by immune-dependent regulation of intestinal cholesterol metabolism. *Eur Heart J* 2022;**43**:518−33.
41. Li Z, Yi CX, Katiraei S, Kooijman S, Zhou E, Chung CK, et al. Butyrate reduces appetite and activates brown adipose tissue *via* the gut−brain neural circuit. *Gut* 2018;**67**:1269−79.
42. Zhuge A, Li S, Lou P, Wu W, Wang K, Yuan Y, et al. Longitudinal 16S rRNA sequencing reveals relationships among alterations of gut microbiota and nonalcoholic fatty liver disease progression in mice. *Microbiol Spectr* 2022;**10**:e0004722.
43. Liu XJ, Duan NN, Liu C, Niu C, Liu XP, Wu J. Characterization of a murine nonalcoholic steatohepatitis model induced by high fat high calorie diet plus fructose and glucose in drinking water. *Lab Invest* 2018;**98**:1184−99.
44. Bárcena C, Valdés-Mas R, Mayoral P, Garabaya C, Durand S, Rodríguez F, et al. Healthspan and lifespan extension by fecal microbiota transplantation into progeroid mice. *Nat Med* 2019;**25**:1234−42.
45. Kleiner DE, Brunt EM, Van Natta M, Behling C, Contos MJ, Cummings OW, et al. Design and validation of a histological scoring system for nonalcoholic fatty liver disease. *Hepatology* 2005;**41**:1313−21.
46. Earle KA, Billings G, Sigal M, Lichtman JS, Hansson GC, Elias JE, et al. Quantitative imaging of gut microbiota spatial organization. *Cell Host Microbe* 2015;**18**:478−88.
47. Amann RI, Binder BJ, Olson RJ, Chisholm SW, Devereux R, Stahl DA. Combination of 16S rRNA-targeted oligonucleotide probes with flow cytometry for analyzing mixed microbial populations. *Appl Environ Microbiol* 1990;**56**:1919−25.

48. Bolger AM, Lohse M, Usadel B. Trimmomatic: a flexible trimmer for illumina sequence data. *Bioinformatics* 2014;**30**:2114−20.
49. Kim D, Langmead B, Salzberg SL. Hisat: a fast spliced aligner with low memory requirements. *Nat Methods* 2015;**12**:357−60.
50. Roberts A, Trapnell C, Donaghey J, Rinn JL, Pachter L. Improving RNA-Seq expression estimates by correcting for fragment bias. *Genome Biol* 2011;**12**:R22.
51. Trapnell C, Williams BA, Pertea G, Mortazavi A, Kwan G, van Baren MJ, et al. Transcript assembly and quantification by RNA-Seq reveals unannotated transcripts and isoform switching during cell differentiation. *Nat Biotechnol* 2010;**28**:511−5.
52. Anders S, Pyl PT, Huber W. Htseq—a python framework to work with high-throughput sequencing data. *Bioinformatics* 2015;**31**: 166−9.
53. Zhuge A, Li S, Yuan Y, Han S, Xia J, Wang Q, et al. Microbiota-induced lipid peroxidation impairs obeticholic acid-mediated anti-fibrotic effect towards nonalcoholic steatohepatitis in mice. *Redox Biol* 2023;**59**:102582.
54. Musso G, Cassader M, Gambino R. Non-alcoholic steatohepatitis: emerging molecular targets and therapeutic strategies. *Nat Rev Drug Discov* 2016;**15**:249−74.
55. Marra F, Svegliati-Baroni G. Lipotoxicity and the gut−liver axis in NASH pathogenesis. *J Hepatol* 2018;**68**:280−95.
56. Kagan VE, Mao G, Qu F, Angeli JP, Doll S, Croix CS, et al. Oxidized arachidonic and adrenic pes navigate cells to ferroptosis. *Nat Chem Biol* 2017;**13**:81−90.
57. Green DR, Galluzzi L, Kroemer G. Cell biology. Metabolic control of cell death. *Science* 2014;**345**:1250256.
58. Day EA, Ford RJ, Steinberg GR. AMPK as a therapeutic target for treating metabolic diseases. *Trends Endocrinol Metab* 2017;**28**: 545−60.
59. Araújo JR, Tazi A, Burlen-Defranoux O, Vichier-Guerre S, Nigro G, Licandro H, et al. Fermentation products of commensal bacteria alter enterocyte lipid metabolism. *Cell Host Microbe* 2020;**27:**358-75.e7.
60. Rizzetto L, Fava F, Tuohy KM, Selmi C. Connecting the immune system, systemic chronic inflammation and the gut microbiome: the role of sex. *J Autoimmun* 2018;**92**:12−34.
61. Tang TWH, Chen HC, Chen CY, Yen CYT, Lin CJ, Prajnamitra RP, et al. Loss of gut microbiota alters immune system composition and cripples postinfarction cardiac repair. *Circulation* 2019;**139**:647−59.
62. Langer HT, Rohm M, Goncalves MD, Sylow L. AMPK as a mediator of tissue preservation: time for a shift in dogma?. *Nat Rev Endocrinol* 2024;**20**:526−40.
63. den Besten G, Bleeker A, Gerding A, van Eunen K, Havinga R, van Dijk TH, et al. Short-chain fatty acids protect against high-fat diet-induced obesity *via* a PPARγ-dependent switch from lipogenesis to fat oxidation. *Diabetes* 2015;**64**:2398−408.
64. Balmer ML, Ma EH, Thompson AJ, Epple R, Unterstab G, Lötscher J, et al. Memory $CD8^+$ T cells balance pro- and anti-inflammatory activity by reprogramming cellular acetate handling at sites of infection. *Cell Metab* 2020;**32:**457-67.e5.
65. Gao X, Lin SH, Ren F, Li JT, Chen JJ, Yao CB, et al. Acetate functions as an epigenetic metabolite to promote lipid synthesis under hypoxia. *Nat Commun* 2016;**7**:11960.
66. Si J, Kang H, You HJ, Ko G. Revisiting the role of *Akkermansia muciniphila* as a therapeutic bacterium. *Gut Microbes* 2022;**14**:2078619.
67. Kim JS, Kang SW, Lee JH, Park SH, Lee JS. The evolution and competitive strategies of *Akkermansia muciniphila* in gut. *Gut Microbes* 2022;**14**:2025017.
68. Kowdley KV, Belt P, Wilson LA, Yeh MM, Neuschwander-Tetri BA, Chalasani N, et al. Serum ferritin is an independent predictor of histologic severity and advanced fibrosis in patients with nonalcoholic fatty liver disease. *Hepatology* 2012;**55**:77−85.
69. Folgueras AR, Freitas-Rodríguez S, Ramsay AJ, Garabaya C, Rodríguez F, Velasco G, et al. Matriptase-2 deficiency protects from obesity by modulating iron homeostasis. *Nat Commun* 2018;**9**:1350.
70. Bazinet RP, Layé S. Polyunsaturated fatty acids and their metabolites in brain function and disease. *Nat Rev Neurosci* 2014;**15**:771−85.
71. Chen X, Kang R, Kroemer G, Tang D. Broadening horizons: the role of ferroptosis in cancer. *Nat Rev Clin Oncol* 2021;**18**:280−96.
72. Wang S, Moustaid-Moussa N, Chen L, Mo H, Shastri A, Su R, et al. Novel insights of dietary polyphenols and obesity. *J Nutr Biochem* 2014;**25**:1−18.
73. Hopiavuori BR, Anderson RE, Agbaga MP. Elovl4: very long-chain fatty acids serve an eclectic role in mammalian health and function. *Prog Retin Eye Res* 2019;**69**:137−58.
74. Koletzko B, Reischl E, Tanjung C, Gonzalez-Casanova I, Ramakrishnan U, Meldrum S, et al. FADS1 and FADS2 polymorphisms modulate fatty acid metabolism and dietary impact on health. *Annu Rev Nutr* 2019;**39**:21−44.
75. Doll S, Proneth B, Tyurina YY, Panzilius E, Kobayashi S, Ingold I, et al. ACSL4 dictates ferroptosis sensitivity by shaping cellular lipid composition. *Nat Chem Biol* 2017;**13**:91−8.
76. Stockwell BR, Friedmann Angeli JP, Bayir H, Bush AI, Conrad M, Dixon SJ, et al. Ferroptosis: a regulated cell death nexus linking metabolism, redox biology, and disease. *Cell* 2017;**171**:273−85.
77. Shimada K, Skouta R, Kaplan A, Yang WS, Hayano M, Dixon SJ, et al. Global survey of cell death mechanisms reveals metabolic regulation of ferroptosis. *Nat Chem Biol* 2016;**12**:497−503.
78. Wang X, Chen X, Zhou W, Men H, Bao T, Sun Y, et al. Ferroptosis is essential for diabetic cardiomyopathy and is prevented by sulforaphane *via* AMPK/NRF2 pathways. *Acta Pharm Sin B* 2022;**12**:708−22.
79. Shi M, Yue Y, Ma C, Dong L, Chen F. Pasteurized *Akkermansia muciniphila* ameliorate the LPS-induced intestinal barrier dysfunction *via* modulating AMPK and NF-κB through TLR2 in Caco-2 cells. *Nutrients* 2022;**14**:764.
80. Yang Z, Kahn BB, Shi H, Xue BZ. Macrophage α1 AMP-activated protein kinase (α1AMPK) antagonizes fatty acid-induced inflammation through SIRT1. *J Biol Chem* 2010;**285**:19051−9.
81. Álvarez-Guardia D, Palomer X, Coll T, Davidson MM, Chan TO, Feldman AM, et al. The p65 subunit of NF-κB binds to PGC-1α, linking inflammation and metabolic disturbances in cardiac cells. *Cardiovasc Res* 2010;**87**:449−58.
82. Wang YQ, Chang SY, Wu Q, Gou YJ, Jia L, Cui YM, et al. The protective role of mitochondrial ferritin on erastin-induced ferroptosis. *Front Aging Neurosci* 2016;**8**:308.
83. Barcelo A, Claustre J, Moro F, Chayvialle JA, Cuber JC, Plaisancié P. Mucin secretion is modulated by luminal factors in the isolated vascularly perfused rat colon. *Gut* 2000;**46**:218−24.
84. Peng L, Li ZR, Green RS, Holzman IR, Lin J. Butyrate enhances the intestinal barrier by facilitating tight junction assembly *via* activation of AMP-activated protein kinase in Caco-2 cell monolayers. *J Nutr* 2009;**139**:1619−25.
85. Hellman L, Rosenfeld RS, Gallagher TF. Cholesterol synthesis from C^{14}-acetate in man. *J Clin Invest* 1954;**33**:142−9.
86. Wiltrout DW, Satter LD. Contribution of propionate to glucose synthesis in the lactating and nonlactating cow. *J Dairy Sci* 1972;**55**:307−17.
87. Araújo JR, Tazi A, Burlen-Defranoux O, Vichier-Guerre S, Nigro G, Licandro H, et al. Fermentation products of commensal bacteria alter enterocyte lipid metabolism. *Cell Host Microbe* 2020;**27:**358-75.e7.
88. Currais A, Kepchia D, Liang Z, Maher P. The role of AMP-activated protein kinase in oxytosis/ferroptosis: protector or potentiator?. *Antioxid Redox Signal* 2022;**37**:115−34.
89. Lee H, Zandkarimi F, Zhang Y, Meena JK, Kim J, Zhuang L, et al. Energy-stress-mediated AMPK activation inhibits ferroptosis. *Nat Cell Biol* 2020;**22**:225−34.
90. Song X, Zhu S, Chen P, Hou W, Wen Q, Liu J, et al. AMPK-mediated BECN1 phosphorylation promotes ferroptosis by directly blocking system X_c^- activity. *Curr Biol* 2018;**28:**2388-99.e5.
91. Bajaj JS, Kakiyama G, Savidge T, Takei H, Kassam ZA, Fagan A, et al. Antibiotic-associated disruption of microbiota composition and function in cirrhosis is restored by fecal transplant. *Hepatology* 2018; **68**:1549−58.

92. Nie K, Ma K, Luo W, Shen Z, Yang Z, Xiao M, et al. Roseburia intestinalis: a beneficial gut organism from the discoveries in genus and species. *Front Cell Infect Microbiol* 2021;**11**:757718.
93. Pichler MJ, Yamada C, Shuoker B, Alvarez-Silva C, Gotoh A, Leth ML, et al. Butyrate producing colonic clostridiales metabolise human milk oligosaccharides and cross feed on mucin *via* conserved pathways. *Nat Commun* 2020;**11**:3285.
94. Yu Y, Jiang L, Wang H, Shen Z, Cheng Q, Zhang P, et al. Hepatic transferrin plays a role in systemic iron homeostasis and liver ferroptosis. *Blood* 2020;**136**:726−39.
95. Lin F, Chen W, Zhou J, Zhu J, Yao Q, Feng B, et al. Mesenchymal stem cells protect against ferroptosis *via* exosome-mediated stabilization of slc7a11 in acute liver injury. *Cell Death Dis* 2022;**13**:271.
96. Kisseleva T, Brenner D. Molecular and cellular mechanisms of liver fibrosis and its regression. *Nat Rev Gastroenterol Hepatol* 2021;**18**: 151−66.
97. Zhang Z, Yao Z, Wang L, Ding H, Shao J, Chen A, et al. Activation of ferritinophagy is required for the RNA-binding protein ELAVL1/HuR to regulate ferroptosis in hepatic stellate cells. *Autophagy* 2018;**14**: 2083−103.